Chapter 3

Expanding genetic studies to cellular phenotypes: analytical exploration of neutrophil function phenotypes

Collaboration Note

The neutrophil function experiments were performed by Kate Waller, Carly Kempster, Harriet McKinney and Joana Batista under the supervision of Kate Downes at the NHS Blood and Transplant Unit, Addenbrookes Hospital. The project was also coordinated by Willem Ouwehand, Department of Haematology and Nicole Soranzo, Wellcome Trust Sanger Institute.

The discovery cohort genotyping data from the Cambridge BioResource was analysed and processed by Heather Elding at the Wellcome Trust Sanger Institute. The whole-genome sequence data was analysed as part of the BLUEPRINT consortium (Chen et al., 2016a).

Analysis of these data was performed in close partnership and supervised by Klaudia Walter (Wellcome Trust Sanger Institute). Klaudia also analysed the genotype data for the Sanquin replication cohort and devised the custom scripts to calculate the parameters from the real-time data. All the other analyses described here otherwise were performed by myself.

Taco Kuijpers and Judy Geissler (Sanquin Research, The Netherlands) coordinated the Sanquin replication cohort, which was genotyped at the Wellcome Trust Sanger Institute. The replication experiments were performed by Anton Tool at Sanquin Research, The Netherlands. Anton and Taco also provided helpful discussions on the details of the neutrophil function assays and on the approaches to analyse the Cambridge discovery cohort data.

3 Expanding genetic studies to cellular phenotypes: analytical exploration of neutrophil function phenotypes

3.1 Introduction

3.1.1 Neutrophil Biology and central role in immune responses

Neutrophils, or polymorphonuclear leukocytes (PMNs), are the most abundant type of white blood cell, constituting approximately 40-60% of total white blood cells (Wright et al., 2010). Neutrophils are characterised by two distinctive morphologies; the lobulated nucleus and presence of protease-containing granules (Kaplan, 2013) (Figure 3.1). The closely related eosinophils and basophils, together with neutrophils, form the granulocytic family of leukocytes (Amulic et al., 2012). Often the first responders in an immune response, neutrophils deploy antimicrobial functions such as phagocytosis to remove pathogens and cell debris, degranulation to release granular lytic enzymes and the respiratory burst to produce reactive oxygen species (ROS) (Kaplan, 2013, Amulic et al., 2012). In healthy homeostatic conditions, the release of mature neutrophils from the bone marrow must be highly controlled to prevent inadvertent activation and possible tissue damage. During infection when the demand is increased, high numbers of neutrophils are released (Amulic et al., 2012).

Neutrophils are technically complex to study being refractory to techniques such as transfection and RNA knock-down. In addition, as terminally differentiated cells they cannot be grown in tissue culture (Amulic et al., 2012). Many insights have been gleaned from either *in vitro* assessment, cell-line models (as discussed in Chapter 2) or mouse models. There are certain differences between murine and human PMNs that can complicate findings. For example, there is a lower number of circulating neutrophils in mice compared to humans (Amulic et al., 2012).

Neutrophils were traditionally thought of as short-lived cells (6-8 hours), incapable of further expansion (terminally-differentiated) and therefore were assumed to play a more passive role in responding to activating signals (Wright et al., 2010, Amulic et al., 2012). However, it is now known that activated neutrophils possess the ability to perform most regulatory or immune-related functions possessed by macrophages, particularly when neutrophils are primed and have longer life spans (Wright et al., 2010). When stimulated, neutrophils can synthesise pro-inflammatory mediators, present antigen through MHC class II receptors to T lymphocytes as well as mediate extensive immune cell cross-talk as summarised in Figure

3.1 (Wright et al., 2010). Below, I discuss in detail the neutrophil functional responses relevant to this chapter.

Neutrophil activation occurs via two-stages. First, resting circulating neutrophils can be "primed" by bacterial compounds and host cytokines and chemokines such as TNF-α, GM-CSF or IFN-γ (Wright et al., 2010). Upon activation, primed neutrophil responses are much greater than those of non-primed activated neutrophils (Hallett and Lloyds, 1995). For example, the gram-negative bacterial outer cell membrane lipopolysaccharides (LPS) prime neutrophils by stimulating the assembly of the NADPH oxidase complex on the membrane. Subsequent stimulation by the bacterial chemoattractant N-formylmethionine-leucyl-phenylalanine (fMLP) then activates the complex (El-Benna et al., 2008). Priming can occur over minutes where pre-formed receptors contained within intracellular granules are mobilized and transported to the plasma membrane. In some cases, over longer periods of transcription further inflammatory molecules can be induced *de novo* (Wright et al., 2010). Full neutrophil activation and mobilisation of all neutrophil killing activities requires integration of multiple environmental signals and is the result of a cascade of activating signalling processes (Amulic et al., 2012).

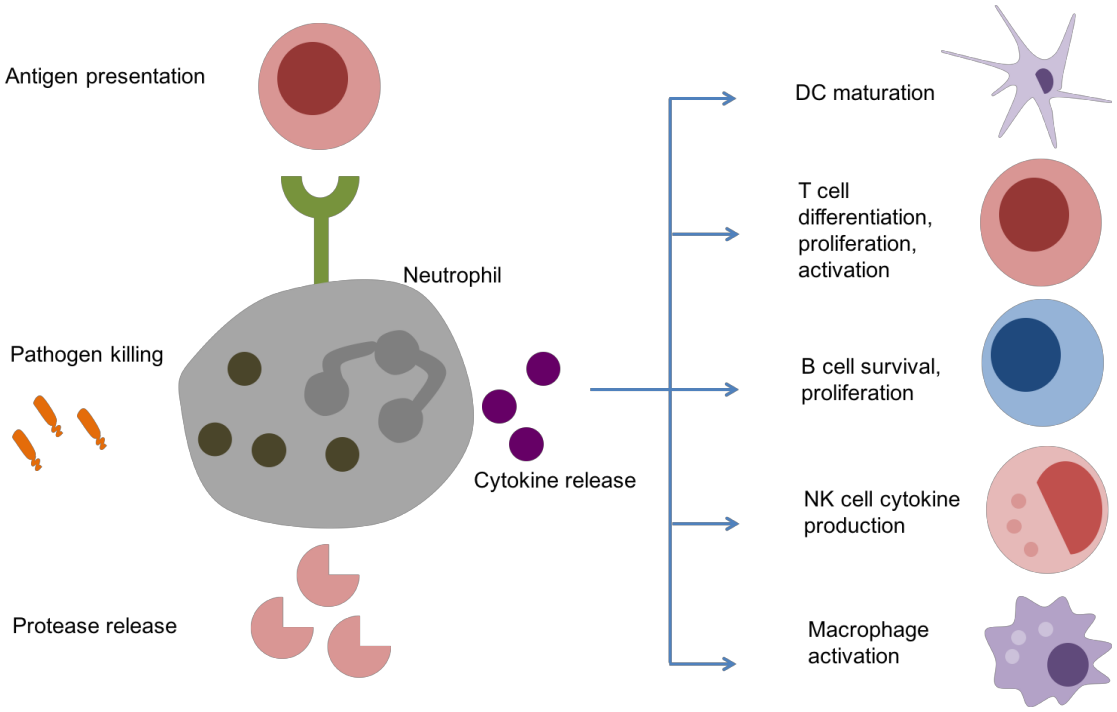

Figure 3.1: The central role of neutrophils in the immune response
Neutrophils are one of the first immune cells to respond to infection and possess a variety of anti-microbial functions. Through cytokine release neutrophils can activate many other cells of the immune system leading to a coordinated adaptive immune response as well as innate response. A relatively new functionality has been observed in the presentation of antigens through MHC class II molecules to elicit T cell activation and proliferation. Some of these functionalities have also been observed to become dysregulated in the pathology of autoimmune disorders. Adapted from (Wright et al., 2014).

Neutrophil activation requires the recruitment of these cells to inflamed tissues, which is achieved through neutrophil recognition of stimulated endothelial cells. Signals derived from either bacterial (LPS and fMLP) or host mediators (TNF-α, IL-1β, Il-17) stimulate the surrounding endothelial cells to express selectin adhesion molecules and members of the integrin super-family, intercellular-adhesion molecules (ICAMs) (Figure 3.3) (Amulic et al., 2012, Borregaard, 2010). Tethering of neutrophils to activated endothelial cells is mediated through neutrophil surface molecules, P-selectin glycoprotein ligand-1 (PSGL-1) and L-selectin, which interact with the endothelial-expressed P- and E-selectins (Figure 3.3) (McEver and Cummings, 1997, Amulic et al., 2012). Neutrophils then roll along the endothelial wall with concomitant activation of signalling kinases including Src family kinases (Syk), phosphoinositide 3-kinase (PI3K) and p38 mitogen-activated protein kinase (Mueller et al., 2010, Amulic et al., 2012). Firm adhesion and the arrest of rolling occurs through integrin contact mediated by the neutrophil-expressed LFA-1 and Mac-1 receptors. Combined with activation by cytokines and chemoattractants, sustained interactions generate changes in neutrophil morphology and a process known as cell spreading (Figure 3.3) (Sengupta et al.,

2006). Cytoskeleton rearrangements enable neutrophils to move along chemotactic gradients. At this stage, the respiratory burst is initiated (Amulic et al., 2012). Firm adhesion allows neutrophils to cross the cell membrane once they reach an endothelial cell junction in a process known as transendothelial migration (Figure 3.3). Neutrophil adherence to the endothelial surface is referred to as adhesion and is a vital step in recruiting neutrophils to the site of inflammation ensuring effector functions are appropriately stimulated reducing the risk of spurious tissue damage.

At the site of inflamed tissue, further host and bacterial inflammatory signals activate the later stages of neutrophil activation. Chemoattractants signalling through GPCRs, such as the fMLP receptor, activate the MAPK/ERK signalling cascade culminating in the assembly of the respiratory burst complexes (Zarbock and Ley, 2008, Selvatici et al., 2006). The NADPH oxidase complex is a multi-protein complex that catalyses the production of powerful oxidising agents known as ROS (Figure 3.4) (Segal et al., 2000). ROS are directly antimicrobial but can also modify host molecules and responses and also influence the activity of granule proteins (Amulic et al., 2012).

Sustained activation by chemoattractants along a chemical gradient also stimulates degranulation, which is the release of antimicrobial contents from the specialised organelles known as granules (Table 3.1). Granules are formed throughout the differentiation process, and their contents vary based on the changing transcriptional programme during development (Amulic et al., 2012). Granules fuse with either the plasma membrane or phagosome, releasing the antimicrobial contents and permanently changing the composition of those membranes (Amulic et al., 2012). Granule deployment has important functional consequences. For example, the specific granules (Table 3.1) contain with flavocytochrome b558, which is a component of the NADPH and therefore, the fusion of these granules with the phagosomal or plasma membrane promotes the respiratory burst response (Amulic et al., 2012, Uriarte et al., 2011). Antimicrobial proteins can be categorised into three groups: those that bind to microbial membranes, those that possess enzymatic activity and those that deprive microbes of nutrients (Amulic et al., 2012). Some examples are given in Table 3.1.

Activated neutrophils can also release extracellular traps (NETs), which are web-like structures of granule proteins and decondensed chromatin. NETs enable the neutralisation of a wide range of pathogens (Papayannopoulos, 2017, Brinkmann et al., 2004). This particular function is not studied in this chapter, but the dysregulation of this process is known to contribute to the aetiology of inflammatory disorders (Papayannopoulos, 2017).

Granule protein	Granule Type	Function
Myeloperoxidase (MPO)	Azurophillic/primary	Can react with H_2O_2 to produce ROS including hypohalous acids
Lysozyme	Azurophillic/primary, Specific (secondary)	Degrades bacterial cell wall
Elastase, Cathepsin G	Azurophillic/primary	Cleaves bacterial virulence factors and outer membrane proteins, binds to bacterial membranes
Defensin	Azurophillic/primary	Arginine-rich cationic peptides, antimicrobial often by disrupting bacterial membranes
Laminin receptor	Specific (secondary), Gelatinase (tertiary)	Cell surface receptor, important for cell adhesion. Binds laminin, an extracellular matrix protein
Bactericidal/permeability-increasing protein (BPI)	Azurophillic/primary	Binds to LPS and increased bacterial permeability and bacterial phospholipid hydrolysis
Azurocidin	Azurophillic/primary	Binds to bacterial membranes
Lactoferrin	Specific (secondary)	Binds to and sequesters iron, which is a bacterial nutrient and inhibits bacterial growth. Binds to lipid A of LPS resulting in a release of LPS from the membrane and increased in permeability
Cytochrome b_{558}	Specific (secondary), Gelatinase (tertiary), Secretory	Component of phagocyte NADPH oxidase
fMLP receptor	Specific (secondary), Gelatinase (tertiary), Secretory	Receptor for bacterial chemoattractant fMLP
MAC-1 (CD11b/CD18)	Specific (secondary), Gelatinase (tertiary), Secretory	Complement receptor
Gelatinase	Specific (secondary)	Gp91phox/p22phox, CD11b, MMP25, arginase-1, β2-microglobulin, CRISP3
Complement receptor 1 (CR1)	Secretory	Complement receptor
LFA-1 (CD11a/CD18)	Secretory	Integrin important for adhesion
Proteinase 3 (PR3)	Azurophillic/primary	Serine protease

Table 3.1: Examples of granule proteins, which granule(s) they are contained within and the function

This table describes the four different types of granules and examples of granule protein content. The four granules include azurophilic, specific, gelatinase and secretory. The list is not exhaustive and there are other proteins contained in neutrophil granules. Exocytosis of neutrophil granules is an important process in activation in response to a stimulus and the destruction of phagocytosed pathogens. This table was adapted from (Amulic et al., 2012, Wright et al., 2010, Nelson et al., 2008).

3.1.2 Neutrophils and disease

Fully functional neutrophil responses are important for appropriate immune responses, which is clearly shown by the inability to fight infections due to defects in neutrophil activation and function in patients with certain primary immunodeficiencies (Bouma et al., 2010, Record et al., 2015). Mutations found in chronic granulomatous disease patients result in a non-functional NADPH oxidase and deficient ROS production (Gennery, 2017, Segal et al., 2000). As a result, these patients are susceptible to severe infection and autoinflammation (Gennery, 2017, Segal et al., 2000, Amulic et al., 2012).

In Chapter 2, I also highlight examples where neutrophil function has been linked to complex diseases. Indeed, dysregulated neutrophil function is a key factor in the pathogenesis of certain inflammatory diseases, highlighting the importance of regulating neutrophil activity to balance effective immune responses while limiting damage to the host (Gupta and Kaplan, 2016). Apoptosis of activated neutrophils is important in the return to homeostatic conditions after an inflammatory response (Wright et al., 2010). Failure of neutrophil apoptosis or deficient clearance of neutrophil apoptotic particles can cause chronic inflammation as observed for example, in chronic obstructive pulmonary disease (COPD) and rheumatoid arthritis (RA) (Amulic et al., 2012, Wright et al., 2010). Neutrophil products, such as MPO and PR3 (Table 3.1) are also known targets of autoantibodies, referred to as antineutrophil cytoplasmic antibodies (ANCA) and have been detected for example in the systemic autoimmune disease, antineutrophil cytoplasmic antibody (ANCA)-associated vasculitis (AAV) (Gupta and Kaplan, 2016). The interaction of ANCAs with antigens on primed neutrophils can activate neutrophil effector processes as described above (Kaplan, 2013). Observations of the presence of ANCAs, activated neutrophils in the synovial fluid and granulocyte-dependent cartilage damage in RA patients also support a role for neutrophil dysregulation in this disease (Emery et al., 1988, Mohr and Wessinghage, 1978, Kaplan, 2013). Indeed, neutrophils from RA patients in remission showed lowered adhesion and chemotactic characteristics, suggesting that migration to the synovial fluid may contribute to disease severity (Dominical et al., 2011).

Beyond autoimmune diseases, there is a well-known association between inflammation and cancer, and neutrophils are present in high numbers in tumours where their infiltration is linked a worse prognosis (Jensen et al., 2009, Amulic et al., 2012). I also discussed the potential role of neutrophils in Alzheimer's disease in Chapter 2 and more widely the contribution of inflammation to other complex diseases including coronary artery disease and age-related macular degeneration.

3.1.3 Functional phenotypes

The observed dysregulation of neutrophil function in multiple immune disorders makes the therapeutic targeting of these functions attractive. Understanding the mechanisms of neutrophil function and how these processes can lead to host tissues damage is an important step in enabling their therapeutic manipulation (Mayadas et al., 2014). Genetic studies of these cells afford the opportunity to discover new biological pathways involved in function, which could aid the identification of potential intervention targets.

In Chapter 1, I described how this goal is helped by using molecular phenotypes to understand disease- and complex trait-associated loci. Such approaches have already been successfully applied to neutrophils, as I highlighted in Chapter 2 with the BLUEPRINT consortium (Chen et al., 2016a). Another recent study also demonstrated the value of studying stimulated neutrophils by assaying neutrophil gene expression measured using a microarray (Naranbhai et al., 2015). The authors identified that 30% of 9,147 genes tested had at least one significant cis-eQTL (Naranbhai et al., 2015). Interestingly, many of these genes were known to function in central processes in neutrophil biology including differentiation, trafficking, granule formation, cytokine secretion, respiratory burst, phagocytosis and migration (Naranbhai et al., 2015). Some differences were observed with stimulated neutrophils, for example, rs1981760 was an eQTL for *NOD2* in unstimulated neutrophils but regulated the expression of the interferon β gene, *IFNB*, in neutrophils stimulated by the NOD2 ligand muramyl dipeptide (Naranbhai et al., 2015). Interferon β is involved in response to NOD2 activation, showing rs1981760 acts at multiple stages of the NOD2 pathway in resting and activated cells. The variant is associated with the risk of the bacterial disease, leprosy (EA = T) but is protective for Crohn's disease (Naranbhai et al., 2015).

In efforts to gain further insight into immunology and its genetic control, there has been a recent expansion in the type of phenotypes studied using genetic approaches. For example, measuring the immune cell production of cytokines in the blood, which has been shown to be highly heritable (Brodin et al., 2015). Indeed, studying protein-level intermediates provides a comprehensive picture of functional variation, particularly as the previous integration of eQTL and protein (p)QTLs showed that some gene effects are buffered at the protein level (Battle et al., 2015). In Chapter 1, I discussed some examples of genetic studies using cellular phenotypes.

Measuring functional phenotypes in stimulated conditions is particularly important for studying immune function. The observed variation in cytokine responses was higher when blood cells were stimulated by a range of physiological stimuli than when compared to the

resting state (Li et al., 2016a). Combining loci associated with protein-level and molecular phenotypes allows identification of more of the functional steps involved in the pathway from sequence variation to organismal traits. For example, rs11141235 was associated with IL6 levels after *Candida* stimulation and through using gene expression data acquired in PBMCs similarly stimulated, the locus was associated with expression of the gene, *GOLM1*, encoding the Golgi membrane protein 1 (Li et al., 2016a). Using a patient cohort, the authors further demonstrated that the *GOLM1* locus was associated with candidemia, suggesting susceptibility is the result of genetically modulated *GOLM1* gene expression and altered IL6 cytokine production (Li et al., 2016a). This genetic approach, therefore, highlights potential novel genes involved in cytokine responses and infection susceptibility.

Cohorts of functional data, therefore, have demonstrated that it is possible to study natural variation in a wide range of intermediate traits. These allow the identification of variants independently of their effects (or lack of effects) on molecular phenotypes, but also provide additional datasets with which to further annotate variants and move closer to the full description of regulation from variant to disease. As yet, there have been no large-scale efforts aimed at studying neutrophil functional phenotypes, due in large part to the technical complexities associated with working with these cells. However, given the central role of these cells in the immune response, such an approach could be highly impactful in informing our knowledge of neutrophil function.

3.1.4 Aims of this chapter: Investigating neutrophil functional responses

In this chapter, I aimed to build on recent efforts to reproducibly measure immune functions and subsequently identify genetic variants associated with functional readouts in healthy individuals. Rather than using a heterogeneous mix of blood cell types, we aimed to specifically study neutrophil responses, given the importance of these cells and their limited inclusion in genetic studies to date. Further, in generating a complementary neutrophil functional genetic dataset to the already established BLUEPRINT epigenome, we hoped to provide additional information for annotating genetic loci of immune and disease interest (Chen et al., 2016a).

I focused on three neutrophil functional responses that represented key stages in activation of these cells; adhesion, degranulation and respiratory burst (Figures 3.3-3.5). I summarise the study design in Figure 3.2 below. Experimental measurement of these responses was carried out by our collaborators Kate Downes and team at the NHS Blood and Transplant Department. Here, I implemented the analytical exploration of what represented the first application of these traits to larger healthy cohorts, having previously been used to study neutrophils from patients with rare disorders (Anton Tool and Taco Kuijpers, Sanquin

Research, the Netherlands). First, I selected parameters representing biologically meaningful estimates of functional response across the whole cohort. Next, I investigated the technical reproducibility of these assays and the effect of known covariates. I then explored possible biological relationships between these functional phenotypes and last assessed whether any observed variation in the responses can be explained by identified genetic variants.

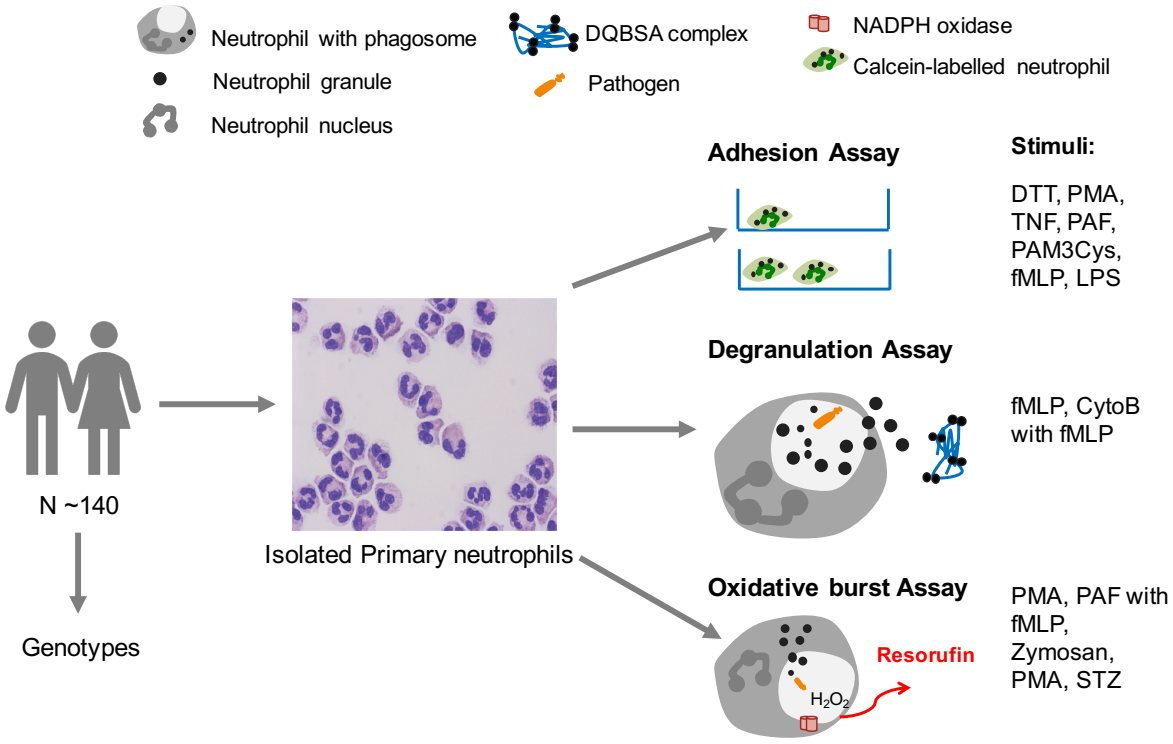

Figure 3.2: Neutrophil function study design
Approximately 200 healthy blood donors were recruited and primary neutrophils were isolated to a high purity (Materials and methods). Three assays were then performed per donor with a range of stimuli to activate neutrophils. DNA was extracted and either processed by whole genome sequencing (part of BLUEPRINT) or genotyped as part of a larger Cambridge BioResource cohort.

3.2 Materials and Methods

3.2.1 Neutrophil function data collection and experimental assays

Neutrophil adhesion, degranulation and respiratory burst were experimentally measured by our collaborators at the NHSBT at Addenbrooke's hospital (Kate Downes and Team). Here, I discuss the technical details of these assays as they are relevant to my quality control analysis and data exploration. To briefly summarise, for each assay fluorescence emitted from different fluorophores was measured for each individual using a plate-reader (Tecan, Infinite F200 PRO), and this represented the strength of neutrophil response.

Sample collection and cell isolation: All sample collection and neutrophil purification was performed at the NHSBT and details of this process are detailed in (Chen et al., 2016a). Briefly, neutrophils were purified from whole blood using a series of Percoll gradients. The resulting cells (neutrophils and eosinophils) were washed, and neutrophils were positively selected using CD16 microbeads (Miltenyi) according to the manufacturer's instructions. An average purity of CD66+CD16+ neutrophils was 98% as assessed by multicolour flow cytometry. Donors were obtained as part of the NIHR Cambridge BioResource (http://www.cambridgebioresource.org.uk/). Peripheral blood samples were collected from healthy donors with informed consent (A Blueprint of blood cells, REC 12/EE/0040, East of England-Hertfordshire Research Ethics committee). After broad outlier exclusion (see below), the cohort consisted of 138 donors where genetic data was available. There were 82 females and 56 males within the cohort. The age of donors ranged from 22 to 75 with 75% of the cohort falling between the ages of 55 and 75. For 87 donors (59%) whole genome sequence data was available as part of the Blueprint consortium cohort and for 102 donors (73%), genotype data from genotyping arrays was available (see below). The data were collected over a period of one year, with between one and four donors measured per day. In 56% of cases, a single donor was measured per day, and in 7% of cases, four donors were measured on the same day. Other exclusions, for example, outliers of the specific assay responses, are explained below.

Adhesion assay: The adhesion assay measures activated neutrophils adhering to a plate as a model system for circulating neutrophils attaching to endothelial cells, a process which is essential for neutrophils to access infected or damaged tissues (Figure 3.3). Neutrophils were first labelled with calcein-AM, supplied in 50 µg/vial. 12.5 µL of DMSO was added to one vial 50 µg vial of calcein-AM. Cells were resuspended in HEPES buffer at 5.0 x 10^6 per ml. 1 µL of the calcein-AM mix was added per ml of cell suspension. The suspension was incubated in a shaking water bath for 30 minutes at 37°C and after 15 minutes tubes were shaken by hand and replaced. 12 mL of PBS was then added and the suspension was centrifuged at 1500 rpm for five minutes, resuspended again in 12 mL of PBS and

centrifugation was repeated as before. Finally, cells were resuspended in HEPES buffer and the concentration determined. For the adhesion assay, a calcein-labelled cell concentration of 2 x 10^6 per mL was used, and 80 µL of cell suspension was added to each well of a 96-well maxisorp plate (Fisher, DIS-971-090X). Eight different stimuli were used in this assay. Final concentrations used to stimulate the neutrophils on the plate were as follows: 1 µM PAF (Sigma, P4904), 10 ng/mL TNF (PeptroTech, 300-01A), 20 µg/mL Pam3Cys (EMC microcollections, L2000) 10mM DTT (Sigma, D0632) 10 µM fMLP (Sigma, F3506), 1 µg/mL PMA (Sigma, P8139), 20 ng/mL LPS (Sigma, L2880) and 50 ng/mL LBP (R&D Systems, 970-LP-025). After addition of the stimulus, the plate was covered with a sealer and incubated in a 37^0C CO_2 incubator for 30 minutes to allow activated neutrophils to adhere to the plastic surface of the plate. Neutrophil adherence to the plate is a known non-specific interaction mediated through the neutrophil integrin receptor, CD11b/CD18, that is blocked by antibodies against CD11b or CD18 (Anton Tool, personal communication). After 30 minutes, non-adherent neutrophils were washed from the plate using 100 µL of PBS at room temperature (RT). 100 µL of 0.5% Triton X-100 (Sigma, T8787) was then added to each well that contained cells, and the plate was incubated at RT for ten minutes. For the 100% input control, 20 µL of 2.5% of Trion X-100 was added to separate wells containing 80 µL of cell suspension. After incubation with Triton X-100, the plate was loaded onto the plate reader and one final fluorescence measurements was recorded. In all three assays, an unstimulated condition with the addition of only HEPES buffer was also measured on the plate reader.

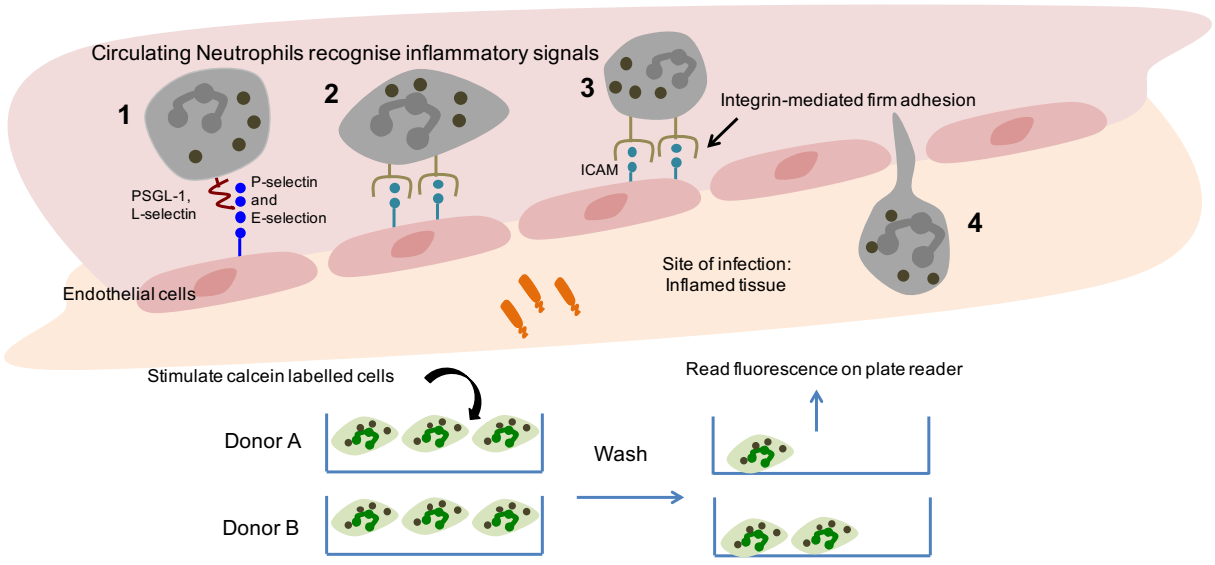

Fig 3.3: Neutrophil adhesion
This schematic shows the biological process of adhesion and experimental measurement (lower panel). Neutrophils are recruited to inflamed tissues described in four-stage process. Initial contact is mediated through selectins (1), initial tethering mediated by the constitutively-expressed neutrophil molecules, PSGL-1 and L-selectin. P-selectin and E-selectin are expressed by endothelial cells under infection or inflammatory conditions. (2) neutrophils then roll along the endothelial wall leading to strong adherence mediated by integrins (3) (Zarbock and Ley, 2008). During the rolling process, other receptor interactions activate further signalling processes in neutrophils to initiate neutrophil extravasation, cytoskeletal rearrangement leading to the release of neutrophil cytotoxic granules and production of reactive oxygen species. The neutrophil crosses the endothelial cell wall in a process known as transendothelial migration (4). To assay this response, neutrophils are labelled with the fluorescent molecule, calcein-AM and activated with the stimuli in the plate well. Fluorescence of adherent neutrophils is measured by a plate reader. Figure adapted from (Amulic et al., 2012).

Respiratory burst assay: This assay measured the NADPH-oxidase activity of neutrophils known as the respiratory burst response. This is the production of reactive oxygen species (ROS) by an activated neutrophil (Figure 3.4). Hydrogen peroxide (H_2O_2) is produced by the neutrophil respiratory burst and reacts with the Amplex® Red reagent in the presence of horseradish peroxidase (HRP) (ThermoFisher Scientific, 2017). The 1:1 reaction of Amplex® Red and H_2O_2 produces the red fluorescent molecule, resorufin (Figure 3.4). Resorufin is excited by 571 nm and emits at 585nm enabling the measurement of the cellular production of H_2O_2 using a plate reader. For this assay, the responses are measured by the plate reader in real-time, rather than an end-point measurement. The fluorescence measured was produced not from labelled cells (as with adhesion) but from the production of fluorescent resorufin as a by-product of the stimulated functional response.

Unlabelled cell concentration used for the respiratory burst assay was 1 x 10^6 cells per mL in HEPES medium. The neutrophil cell suspension was pipetted into a black opaque 96 well plate (Fisher, DIS-210-190W). 100 µL of the 2x reaction mix containing a final concentration of 25 µM Amplex® Red (10-acetyl-3,7-dihydroxyphenozazine, Molecular Probes, A-12212) and 0.5 unit/mL HRP (Sigma, P-8250) was added to the plate along with 50 µL of cell suspension. The plate was then incubated at 37°C on the plate reader for five minutes. 50 µL of each stimulus was then added to the relevant wells, and the reaction is then measured in the plate reader immediately after. There were four stimuli used in the respiratory burst assay and the final concentrations used in the assay are as follows: 4 mg/mL Zymosan (Sigma, Z4250), 1 mg/mL STZ (Sigma, P8139), 1 µg/mL PMA (sigma, P8139), 2.5 µM PAF (Sigma, P4904) and 25 µM fMLP (Sigma, F3506) where PAF and fMLP were added to the same well as one condition. The reaction was measured on the plate reader for 60 cycles (30 minutes). The range of different stimuli, both biological and small chemical molecules are described in Table 3.2 with a description of how these stimuli activate the respective neutrophil functions.

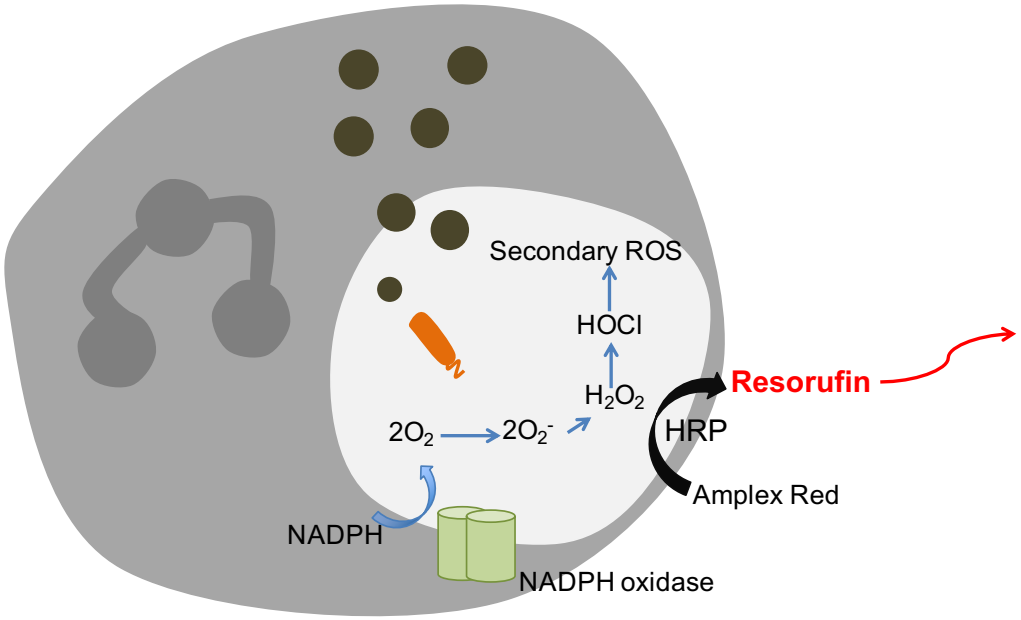

Fig 3.4: The neutrophil respiratory burst response
This schematic summarises the molecular reaction and experimental measurement of the respiratory burst response. Reaction of hydrogen peroxide (H_2O_2) with the Amplex® Red reagent in the presence of horseradish peroxidase (HRP) produces the red fluorescent molecule, resorufin. Resorufin can be excited by 571 nm and emits at 585nm enabling the measurement using a plate reader. Adapted from (Kobayashi et al., 2005).

Degranulation assay: This assay measured the release of granule contents that occurs when a neutrophil is activated (Figure 3.5). Table 3.1 lists the different neutrophil granules and their contents. Here, neutrophil degranulation was measured by using a complex of a DQ^{TM}Green BSA (DQBSA) (Molecular probes, D12050). In this form fluorescence from the green-fluorescent BODIPY® FL dye is quenched (ThermoFisher Scientific, 2017). Proteases released from the neutrophil digest the DQBSA molecule so that the fluorescence is no longer quenched and can be measured by the plate reader. The experimental process mirrors the recognition and internalisation of pathogens by neutrophils that activates a series of molecular processing leading to the release of neutrophil granular contents into the phagosome and also the surrounding cellular environment. The release of antimicrobial peptides and other immune-related molecules leads to the destruction of the pathogen and recruitment of further immune cell types.

HEPES medium was added to the relevant wells in the plate (black opaque 96-well plate as above for respiratory burst assay). 50 µL of unlabelled cells at 5 x 10^6 cells per mL were

added to the wells containing HEPES. A final concentration of 10 µg/mL of DQBSA was added to wells containing cells. For the stimuli, a final concentration of 5 µg/mL Cytochalasin B (CytoB, Sigma, C6762) was used, and 10 µL of this solution was added to the relevant wells containing neutrophil cell suspension and DQBSA. The plate was then incubated for five minutes at 37˚C in the plate reader. The plate was then removed and 10 µM fMLP added to the relevant wells, where neutrophils were stimulated with a combination of CytoB and fMLP. After activation, the released DQ^{TM} Green fluorophores released are excited at 505nm and emit at 515nm. The reaction was measured in the plate reader for 120 cycles (60 minutes).

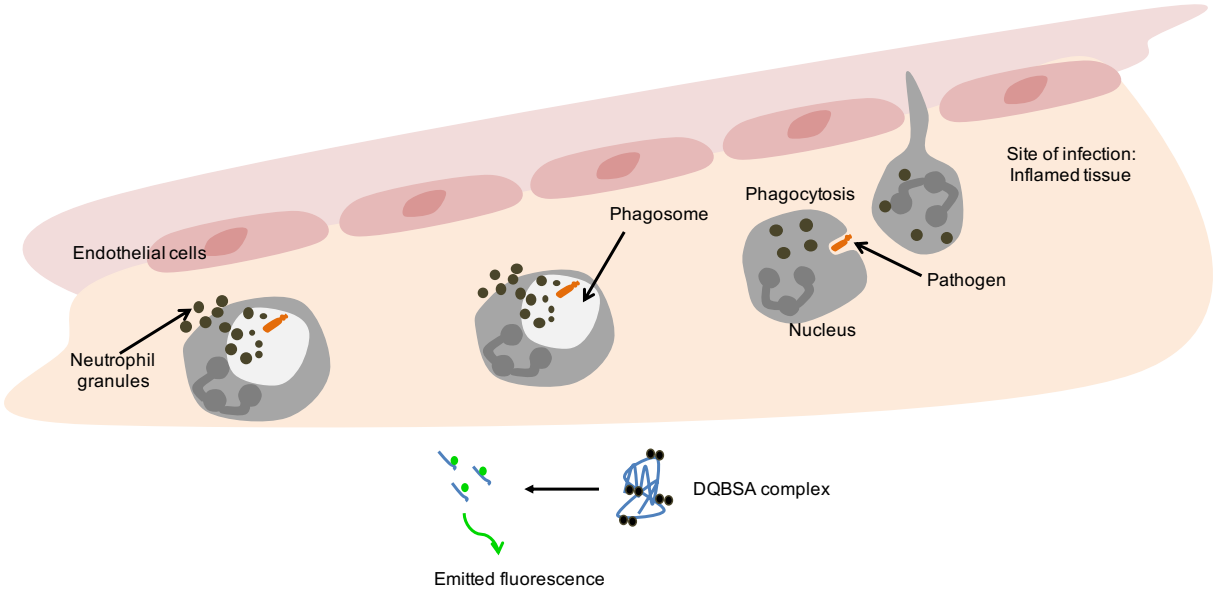

Fig 3.5: Neutrophil degranulation
This schematic shows the biological process and experimental measurement of degranulation, which is the release of granule contents. The response from purified neutrophils in solution is measured using a fluorescent marker. Released neutrophil proteolytic enzymes break up the DQBSA molecule so that DQ is no longer quenched and the fluorescence can be measured using a plate reader. Adapted from (Amulic et al., 2012).

3.2.2 Data interpretation and exploration

Given the novelty of the traits, we carried out extensive exploration of the data to identify potential artefacts. These next sections describe the process used to evaluate the utility of these traits in a genetic context and was carried out with close collaboration and supervision by Klaudia Walter.

Initial exploration of data over time: To assess the variability of the measures over time, I plotted each trait value by date of acquisition across the 12 months. As a first diagnosis, we assessed traits as calculated by and provided by the plate reader software. These were relative fluorescence units measured at cycle 20 and 40 for respiratory burst and degranulation respectively. For adhesion RFU measurement was an end-point value after a 30 minutes incubation (see above). Figure 3.6 also shows the two replicates of the 100% input control used in the adhesion assay and measured for each donor. The 100% input control is the measured calcein fluorescence (in RFU) from labelled cells after addition of a high concentration of Triton-X100 (Materials and Methods), which should release calcein from the cells and reflect a high adhesion response. This value is used to normalise the adhesion response for all other stimuli by dividing the stimulated RFU by the 100% input control (four of the total eight stimuli are shown in Figure 3.6 and listed in Table 3.2).

We observed a substantial shift in trait values and distribution between the first 68 samples and those acquired after this point (Figure 3.6). In particular, for the adhesion response, the HEPES values were inflated compared to the samples acquired later (Figure 3.6). This elevated HEPES response level could reflect possible bacterial contamination in the original HEPES batch, resulting in neutrophil activation. The HEPES buffer was used in all parts of the experimental process including stimulus dilution. Therefore, the decision was taken to remove the first 68 samples.

Selection of real-time assay parameters: One major challenge for the respiratory burst and degranulation real-time assays was the selection of a comparable measurement that can be used as a phenotypic trait for subsequent genetic studies. We explored the raw response distributions to select parameters that would best capture the highest dynamic range in response across the cohort yielding the largest resolution (Figure 3.7).

The shape of the response distributions often varied considerably between stimuli (Figure 3.7). For example, the respiratory burst response stimulated by Zymosan, a yeast particle, shows a slower activation profile than with serum treated Zymosan (STZ). STZ is Zymosan opsonised with immunoglobulin (Ig) and complement receptors that together stimulate a faster and higher neutrophil response by activating the integrin receptor CD11b/CD18.

Addition of Cytochalasin (CytoB) with fMLP also elicits a higher response (Figure 3.7). fMLP stimulates the production of diacylglycerol (DG) by phospholipase C (PLC). DG activates protein kinase C (PKC), a kinase that has been suggested to be involved in both ROS production and degranulation (Sato et al., 2013). CytoB has been shown to increase the diacylglycerol-mediated response stimulated by fMLP in neutrophils and therefore augments the fMLP response (Honeycutt and Niedel, 1986).

We combined the observed reaction distributions with prior knowledge regarding the biological relevance of reaction ranges (Anton Tool, personal communication) to calculate a range of parameters directly from the raw responses for both the respiratory burst and degranulation assays. For example, we were advised that the respiratory burst reaction stimulated by PAF combined with fMLP, is an extremely rapid reaction reaching saturation within minutes. Therefore, we calculated parameters for the PAF & fMLP response within the first ten cycles (five minutes) of the reaction to avoid missing the oxidative burst peak.

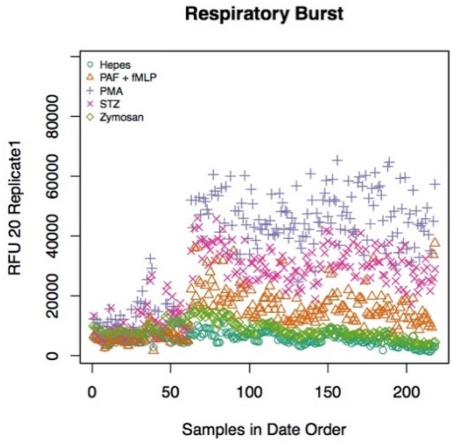
Respiratory Burst
Hepes
PAF + fMLP
PMA
STZ
Zymosan
RFU 20 Replicate1
0
20000
40000
60000
80000
0
50
100
150
200
Samples in Date Order

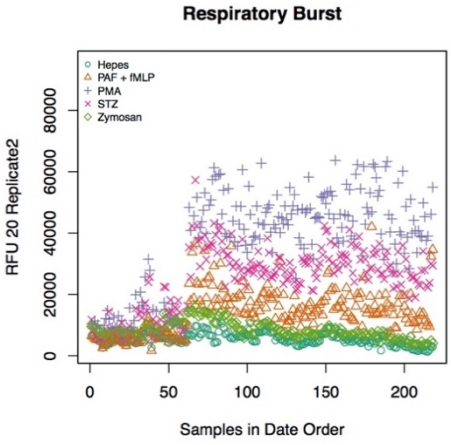
Respiratory Burst
Hepes
PAF + fMLP
PMA
STZ
Zymosan
RFU 20 Replicate2
0
20000
40000
60000
80000
0
50
100
150
200
Samples in Date Order

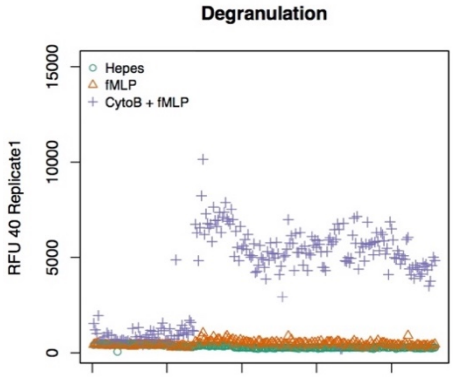
Degranulation
Hepes
fMLP
CytoB + fMLP
RFU 40 Replicate1
0
5000
10000
15000

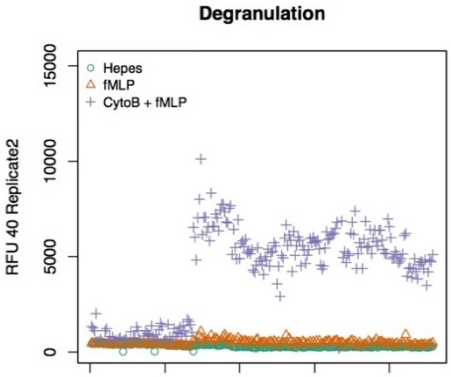
Degranulation
Hepes
fMLP
CytoB + fMLP
RFU 40 Replicate2
0
5000
10000
15000

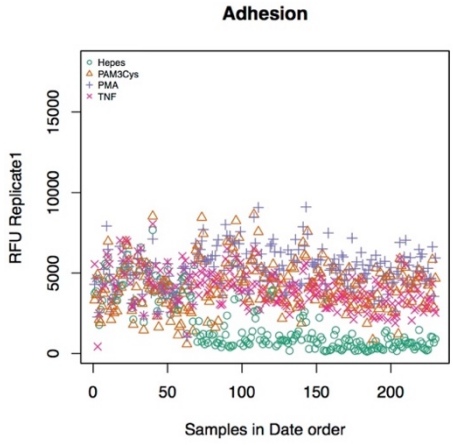
Adhesion
Hepes
PAM3Cys
PMA
TNF
RFU Replicate1
0
5000
10000
15000
0
50
100
150
200
Samples in Date order

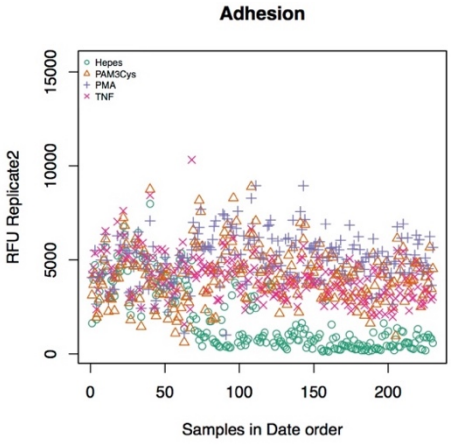
Adhesion
Hepes
PAM3Cys
PMA
TNF
RFU Replicate2
0
5000
10000
15000
0
50
100
150
200
Samples in Date order

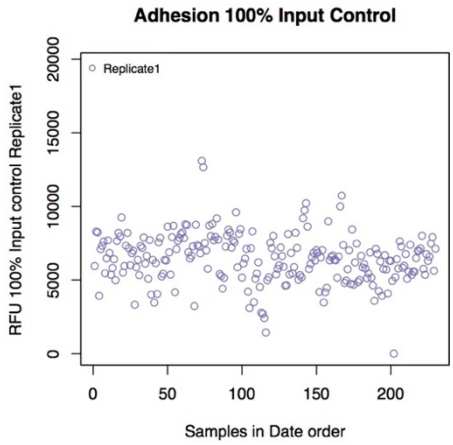
Adhesion 100% Input Control
Replicate1
RFU 100% Input control Replicate1
0
5000
10000
15000
20000
0
50
100
150
200
Samples in Date order

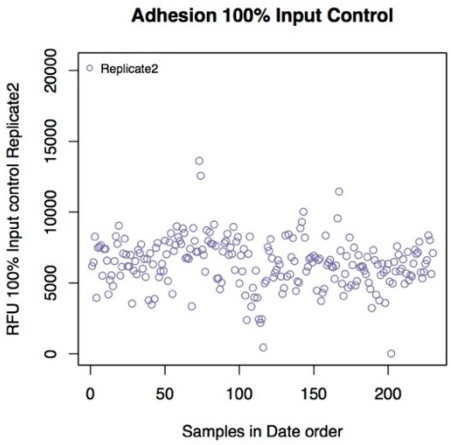
Adhesion 100% Input Control
Replicate2
RFU 100% Input control Replicate2
0
5000
10000
15000
20000
0
50
100
150
200
Samples in Date order

Fig 3.6: Exploratory data analysis: measurements by time
These plots depict the raw data distributions for example RFU values as collected directly by the plate reader software. All donor values for each assay are plotted against the date of acquisition of that sample. The top panel shows an example measurement of the RFU at 20 cycles for all respiratory burst conditions and the second panel shows RFU at 40 cycles for all degranulation conditions. The third panel depicts some example stimuli for the end-point RFU reflecting the degree of neutrophil adhesion on the plate. The fourth panel shows the adhesion 100% input control against date of acquisition. In panels 1-3 it can be observed how the first 68 samples show a very different relative response distribution to the remaining samples.

Figure 3.7 shows that for an individual's response distribution and within each well, there were small fluctuations between successive cycles, particularly apparent for the HEPES degranulation response. These small changes were likely due to plate reader resolution but could potentially have introduced errors in calculating our maximum and mean gradients from the raw distribution. These gradients were used as a comparative measure of the response of each donor in the real-time assays. Mean and maximum gradients were calculated using two successive cycles forming a tangent against the curve for which the gradient was calculated. For mean slope traits within the defined interval, gradients were calculated for each of successive cycles, and the mean was calculated of all these values (all summarised in Table 3.2). To remove these cycle-to-cycle deviations within each individual distribution, we applied the LOESS curve-fitting function to smooth each distribution (Figure 3.7). LOESS is a non-parametric, local regression method, where the fitted points and standard errors are calculated with respect to the whole reaction distribution. An estimated curve is fitted to the reaction distribution curve. This was implemented using the loess() R function. Parameters were then calculated for each replicate separately and then averaged across trait replicates. The function did not effectively fit the PAF fMLP respiratory burst response before cycle 10 (data not shown) due to the rapid reaction in the early cycle-stages resulting in steep response gradients. This rapid reaction also meant that in the early part of the reaction, the response distribution was already smooth and therefore, the raw data without LOESS fitting was used to calculate the parameters for this response. The unsmoothed and smoothed distributions are shown in grey and purple respectively in Figure 3.7.

For adhesion data, there was an extra normalisation step with division of RFU by the 100% input control from the stimuli RFU. Following this, I calculated the averaged across the two technical replicates as described for the other two assays. In total, there were 29 traits across all three assays in the final list of parameters (Table 3.2).

A

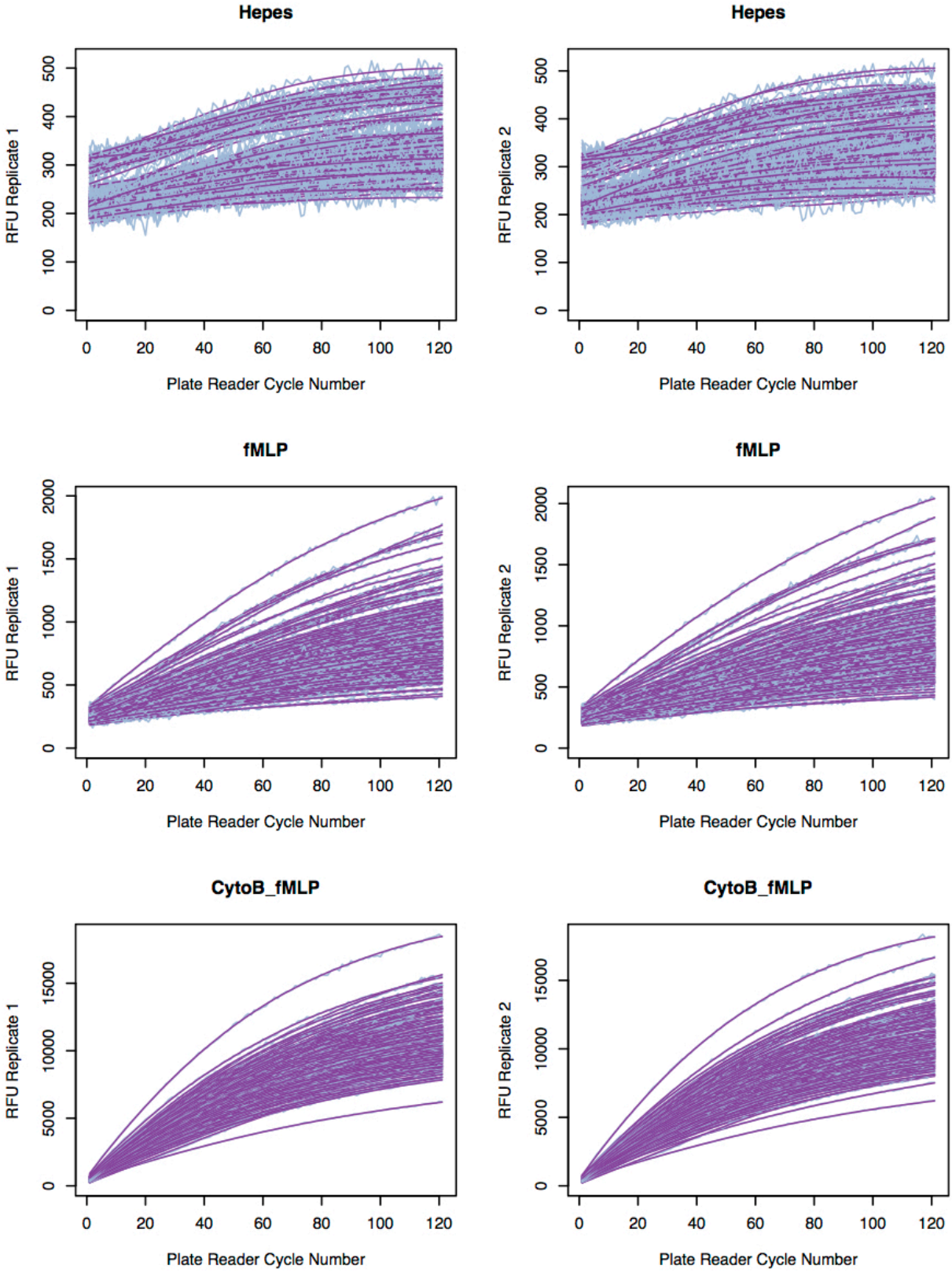
Hepes
RFU Replicate 1
Plate Reader Cycle Number
Hepes
RFU Replicate 2
Plate Reader Cycle Number
fMLP
RFU Replicate 1
Plate Reader Cycle Number
fMLP
RFU Replicate 2
Plate Reader Cycle Number
CytoB_fMLP
RFU Replicate 1
Plate Reader Cycle Number
CytoB_fMLP
RFU Replicate 2
Plate Reader Cycle Number

B

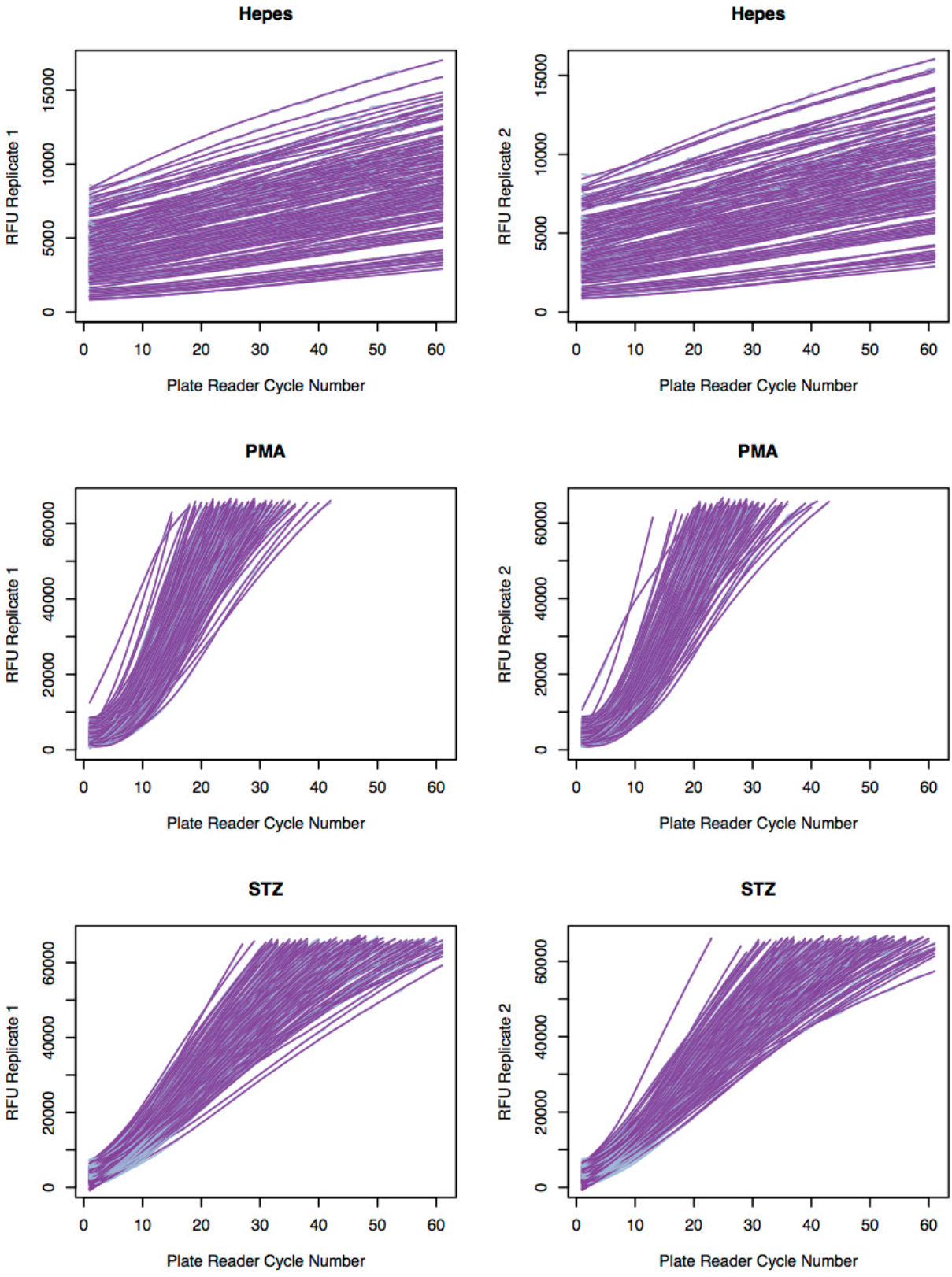
Hepes
RFU Replicate 1
0
5000
10000
15000
0
10
20
30
40
50
60
Plate Reader Cycle Number
Hepes
RFU Replicate 2
0
5000
10000
15000
0
10
20
30
40
50
60
Plate Reader Cycle Number
PMA
RFU Replicate 1
0
20000
40000
60000
0
10
20
30
40
50
60
Plate Reader Cycle Number
PMA
RFU Replicate 2
0
20000
40000
60000
0
10
20
30
40
50
60
Plate Reader Cycle Number
STZ
RFU Replicate 1
0
20000
40000
60000
0
10
20
30
40
50
60
Plate Reader Cycle Number
STZ
RFU Replicate 2
0
20000
40000
60000
0
10
20
30
40
50
60
Plate Reader Cycle Number

C

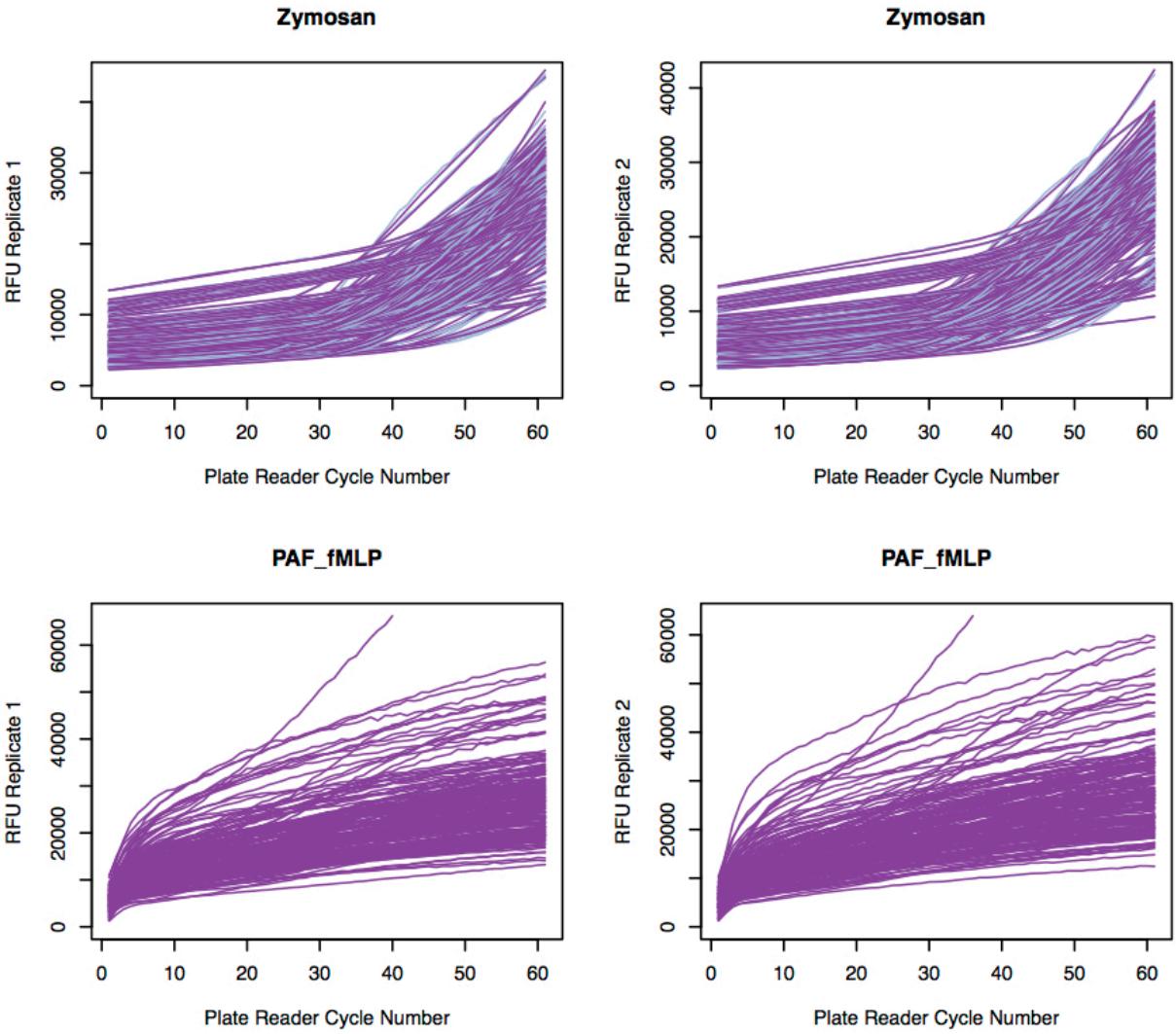

Fig 3.7: Raw data response distributions for respiratory burst and degranulation
These plots show the raw RFU at each cycle for replicate 1 and replicate 2 for every stimulus starting from the first measurement at cycle 1 up to the final number of cycles (60 or 120). Measurements are recorded every 30 seconds (one cycle) plotted on the x-axis. Fluorescence units are measured cumulatively. HEPES buffer is used in each assay as a measure of unstimulated functional response. Each line represents the whole RFU response distribution for one donor. Above is shown the response distributions for all donors in the cohort excluding the first 68 samples. A) Cumulative fluorescence recorded by a plate reader for the degranulation assay for each stimulus used. For the second HEPES replicate there was one donor which recorded a very low HEPES response, near to zero. It was suggested that this could be due to a technical artefact, therefore for this donor, the value for replicate 1 was used in place. B-C) Fluorescence measurements as recorded by a plate reader for the respiratory burst assay for each stimulus used. The raw relative fluorescence values (RFU) from the plate reader are plotted in grey. The values were fitted using the LOESS smoothing function and are shown in purple on the same plot. For respiratory burst responses stimulated by PAF fMLP the plot is shown with raw data. The LOESS function did not fit the raw data well below 10 cycles and so was not used to calculated the trait values. The individual response showing a very different reaction distribution, rising very quickly outside of the other donor responses, in the PAF & fMLP reaction (C bottom panel), was removed (discussed below).

Assay	Stimulus	Trait	N
Respiratory burst	PMA: phorbol myristate acetate, induces NADPH oxidase by direct stimulation of protein kinase C (PKC)	RFU at 10 cycles	130
		RFU at 15 cycles	130
		Time to RFU at 40000 cycles	130
		Mean Slope: 10 to 15 cycles	130
		Maximum Slope	130
	STZ: serum-treated Zymosan, which is opsonised with Ig and complement receptors, involves the neutrophil CD11b/CD18 and Fcγ receptors	RFU at 15 cycles	129
		RFU at 20 cycles	129
		Time to RFU at 30000	129
		Mean Slope: 10 to 20 cycles	129
		Maximum slope	129
	Zymosan: cell wall preparation from *S.cerevisiae,* induces NADPH oxidase via CD11b/CD18	RFU at 60 cycles	130
		Difference in RFU: 60 and 1 cycles	130
		Maximum Slope	130
	PAF + fMLP: PAF amplifies the RB response. fMLP stimulates the fMLP receptor, which activates NADPH oxidase via p47phox	RFU at 6 cycles	127
		Maximum Slope	128
Degranulation	fMLP: N-formyl peptide released by bacteria, bacterial degradation or mitochondrial protein. Stimulates release of gelatinase granules	RFU at 20 cycles	135
		Mean Slope: 20 to 40 cycles	135
		Maximum Slope	135
	Cytochalasin B + fMLP: CytoB, a fungal mycotoxin, inhibits actin polymerisation in cells and amplifies azurophilic and specific granule-mediated degranulation. Generates an increased degranulation response compared to fMLP alone	RFU at 20 cycles	135
		Mean Slope: 20 to 40 cycles	135
		Maximum Slope	137
Adhesion	PMA: activates partially by the stimulation of PKC	Final RFU	131
	PAF: platelet activating factor, binds to the GPCR, PAF receptor	Final RFU	131
	fMLP: activates adhesion through the fMLP receptor	Final RFU	131
	DTT: dithiothreitol reducing agent. Breaks disulphide bridges and activates integrin receptors	Final RFU	129
	TNF: tumour necrosis factor, activates adhesion via the TNF receptor	Final RFU	132
	LBP + LPS: LPS is a bacterial molecule that binds TLR4, LBP is LPS binding protein, an acute phase protein that binds to bacterial LPS to stimulate an immune response	Final RFU	131
	Pam3Cys: TLR1/2 agonist	Final RFU	132
	Hepes: control buffer, may reflect pre-stimulated adhesion	Final RFU	128

Table 3.2: Functional traits and number of individuals for each trait across all three assays and stimuli used
Table describes the different stimuli and their mechanism of action in each assay. The final traits used for each assay is also listed and the number of individuals (N) after final outlier removal within each trait is listed. A full understanding of the signalling pathways involved is not yet established, presented here is a mix of published and unpublished observations from our collaborators (Anton Tool, Taco Kuijpers).

Removal of outliers and technical reproducibility: For each individual, two repeat measurements were acquired where cell suspension from the same donor was added to two wells of the plate (referred to as technical replicates). I used the R function, cor.test to calculate the Spearman correlation between technical replicates across all individuals, for each trait. Before outlier removal the correlation averaged across all traits was high (respiratory burst rho= 0.906, degranulation rho= 0.972, adhesion rho= 0.956), suggesting good technical reproducibility.

I next used these technical replicates to remove outlier measurements or extreme measurements using two thresholds. First, outliers beyond a threshold of 5 x standard deviation (5SD) between technical replicates were excluded. Second, I calculated a 3SD mean *distribution* threshold, to assess potential outliers with very high or low trait values, which could reflect extreme responders or technical artefacts. To differentiate between true high and low responders and technical outliers, I kept measurements that were outside of the mean distribution thresholds but well replicated (inside the 3SD replicate thresholds).

For the adhesion assay, outliers were first excluded using the above thresholds from the un-normalised stimulated RFUs if outside the two thresholds and also from the for raw 100% input RFUs. Finally, outliers were also excluded after normalisation with the 100% input control if this generated additional outliers by normalising with very high or low input control values.

We further investigated four donor measurements that generated very extreme responses that lay far beyond the 3SD mean distribution threshold in most adhesion conditions (data not shown). We identified that these four donors were measured on the same day, the 22nd April 2014 and were the only donors processed using a single batch of a reagent Buffer 3, which is used in the neutrophil purification process. We excluded these donors from further analysis. The extensive investigation into batch effects is discussed below.

I also excluded donors for which there was no available genetic data and then inverse normalised the trait values across the whole cohort to generate a normalised trait distribution.

Covariate investigation: The identification of the four adhesion outliers described above suggested that these functional data may be subject to variation introduced by experimental covariates. We were able to investigate known experimental covariates such as reagent batch as changes were recorded during data acquisition. I also investigated the effect of environmental factors such as age, gender and season. Batch effects, which are sub-groups of trait values that exhibit different behaviour that is not related to genotype, must be

removed to reduce noise, improve power and avoid systematic stratification that can cause bias in association testing (Leek et al., 2010).

In order to investigate the effect of season, we assigned the trait values to the different seasons based on when they were experimentally measured. These included: Winter (Dec-Feb), Spring (Mar-May), Summer (Jun-Aug) and Autumn (Sep-Nov). In addition, if multiple donors were processed on one day (in some cases up to 4), all samples were read on one plate-reader plate and positioned from left to right. The fluorescent signal from each well is also read by the plate reader from the left to right, but the reaction was started once the stimulus was added to the plate prior to placing in the plate reader. We annotated each measurement with plate position to investigate whether machine reading could be a source of co-variation.

I stratified trait values by these potential covariates to visualise the potential effect and Figure 3.8 shows these effects for the adhesion traits as an example. I used inverse-normalised trait values after removal of donor outliers and donors with missing genotypes, to allow better comparison between traits. Patterns for inverse normalised and raw data were similar (data not shown). I calculated the significance of the effect of the covariate by using the one-way ANOVA, using the aov R function, to test if the means of each group were significantly different (shown in Figure 3.8). Certain covariates, such as buffer 3 significantly affected all traits from all three assays, except adhesion PAF (p value = 0.091) and respiratory burst PMA Time to RFU 40000 (p value = 0.11) (Figure 3.8). As described above, buffer 3, was used in the purification of neutrophils from whole blood and also had multiple batches.

I observed that some covariates, such as season, showed variable significance across the different traits. In the case of adhesion, season has a significant effect on the response stimulated by LBP and LPS (p value = 1.6×10^{-07}), HEPES (p value = 7.6×10^{-07}), TNF (p value = 8.6×10^{-03}) and DTT (p value = 2.2×10^{-03}) but not Pam3Cys (p value = 0.18), PAF (p value = 0.25), PMA (p value = 0.15) or fMLP (p value = 0.65). The LBP/LPS response, for example, was lower in winter than it was in spring. LPS is the major component of gram-negative bacterial outer membranes, eliciting an anti-bacterial neutrophil response. In addition, the HEPES response, which may represent the pre-stimulated neutrophil adhesion response was also lower in winter. For the respiratory burst, season as a significant effect on PMA RFU.10 ($p = 6.3 \times 10^{-05}$), PMA RFU 15 ($p = 8.2 \times 10^{-03}$), STZ RFU 15 ($p = 4.4 \times 10^{-06}$), STZ RFU 20 ($p = 2.2 \times 10^{-04}$), STZ Time to RFU 30000 ($p = 6.9 \times 10^{-04}$), PAF + fMLP ($p = 6.5 \times 10^{-06}$), Zymosan RFU 60 ($p = 1.0 \times 10^{-11}$), Zymosan Diff RFU 1.60 (p value = 2.2×10^{-19}) and Zymosan max slope ($p = 8.2 \times 10^{-17}$). For these traits, the pattern was similar to adhesion, highest levels in summer, followed by spring and lowest in winter. For the

degranulation response, season was a significant effect on all traits, with the peak response in spring and decreasing in winter (data not shown).

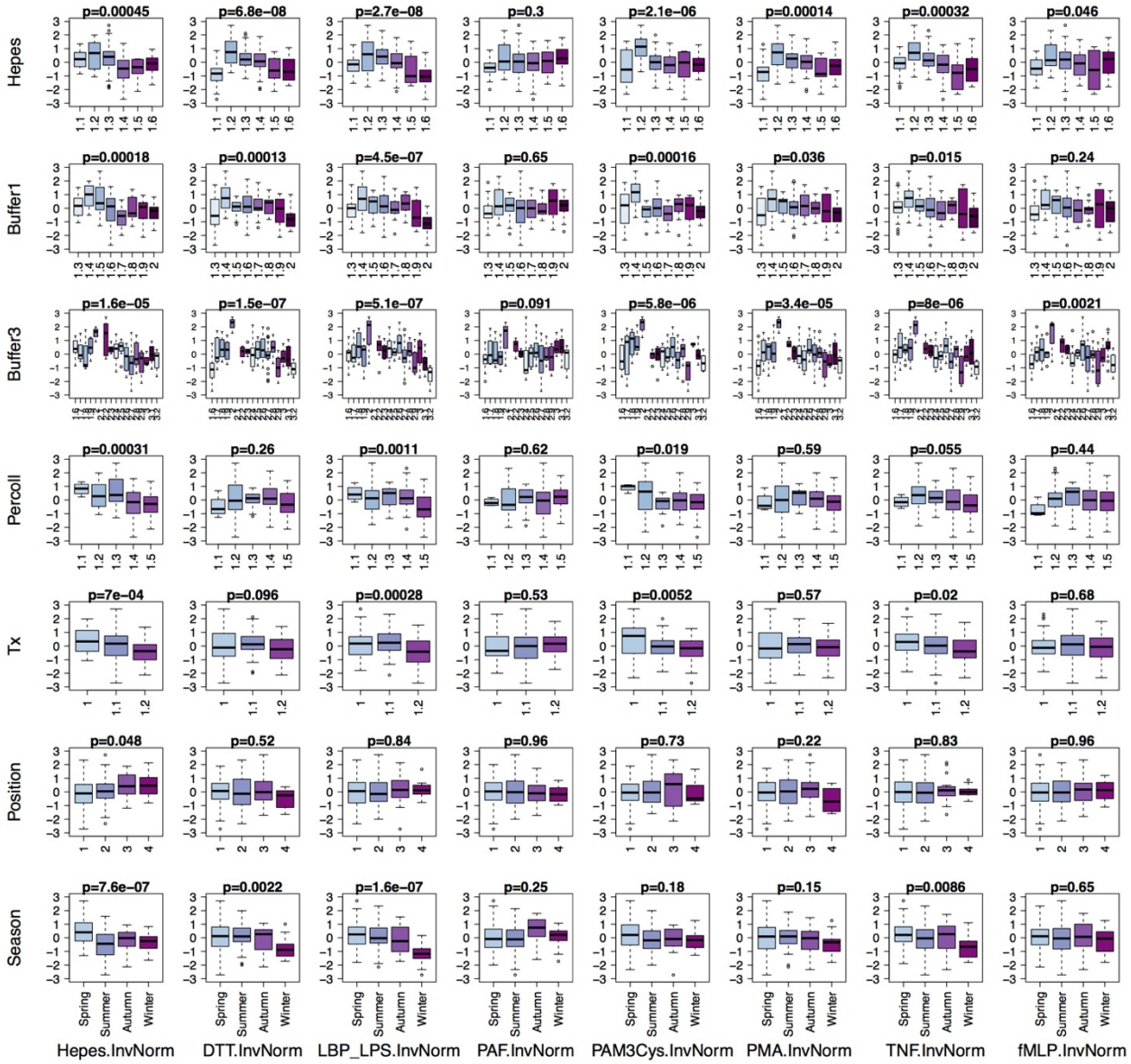

Figure 3.8: Reagent batch effect has a substantial effect on adhesion data
Inverse normalised trait values for neutrophil adhesion stimulated by a variety of stimuli (columns) are shown stratified by covariate levels (rows). HEPES, buffer1, buffer 3 and Percoll are all used in the purification of neutrophils. Triton (Tx) is used in the input control and in the main assay processing. Position explains the position of the donor cells in the well depending on the number of donors assayed. Season is the time of year at which the measurement was acquired.

To further evaluate the effect of each covariate on trait values, I calculated the R^2 value, which determines the percentage of the variation in response that is explained by the model. It is calculated by dividing the variation explained by the model by the total variation. The higher the R^2, the more trait variation is explained by the model. For each trait, I calculated the R^2 value for a linear model where the trait was the response variable and each covariate was fitted independently as the predictor variable. Here, R^2 is expressed as a percentage of trait variation where 0.1 is 10%. Figure 3.9 shows an example of R^2 of covariation for adhesion responses and the remaining traits in Supplementary Figure 3.9.

Reagent batch, particularly that of the neutrophil purification buffers 1 and 3 explain a high proportion of the total variation in each neutrophil trait value. The R^2 averaged across all traits from all three assays was 0.385 and 0.306 for buffer 3 and buffer 1 respectively. These high values underline the considerable effect that reagent batch had on these functional readouts. Interestingly, for all traits, season (mean $R^2 = 0.163$) demonstrated a greater R^2 than age (mean $R^2 = 0.029$) and gender (mean $R^2 = 0.036$) of the donor, suggesting that season contributes a reasonable degree of trait variation. In addition, age was not a significant covariate for any of the traits tested. The observation of the effect of reagent batch and to a certain extent, season, has important implications for the experimental design of future studies involving these cellular functional responses.

Covariate correction: Various approaches for correcting for these covariates were explored, but were often complicated by limited sample size (Klaudia Walter, data not shown). We decided to implement a conservative approach in correcting for covariates given the small sample size of this study, the large observed reagent batch effects and the lack of a complete, genome-wide replication cohort. We included all of the covariates in the trait correction process, termed the “full model”. This approach should lead to the lowest number of false positive associations in the downstream genetic analysis, as opposed to correcting only for those covariates with a significant ANOVA p-value or high R^2 value.

I used linear regression to correct for the technical variation related to these factors. Covariates were input as fixed effects and regressed onto the inverse normalised trait values using the R lm() function. The model fit was assessed using QQ plots (data not shown) and visualisation of the residuals both against time and stratified by covariates to assess whether the previous patterns and waves of variation were still present in the data. We concluded that the residuals generated from the linear regression demonstrated that a considerable proportion of the variation in the response had been removed (Figure 3.10). The mean of the trait values of each covariate batch was now similar, and the varying distribution of values has been removed (Figure 3.10).

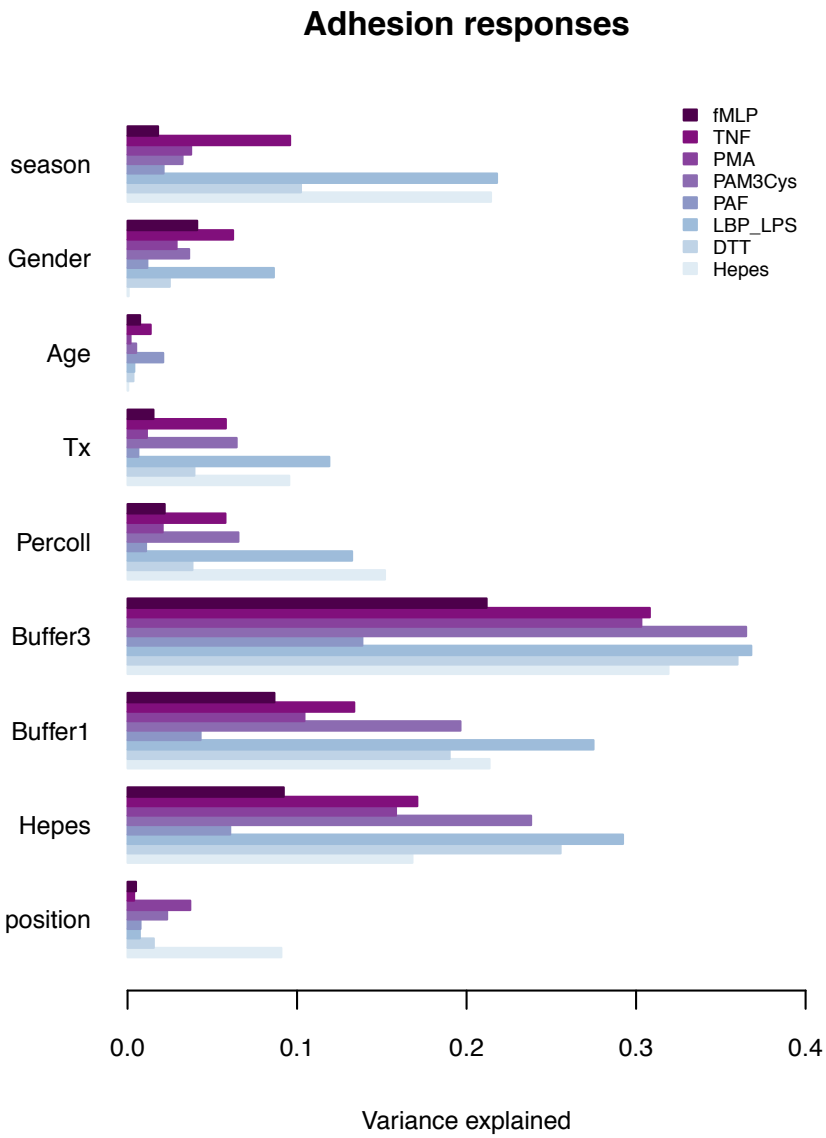

Figure 3.9: Reagent batch explains a high proportion of variation in neutrophil adhesion responses
Barplot shows the R^2 estimates calculated from fitting a linear model for each trait (coloured) independently with each covariate (y axis). This shows that reagent batch explains a high proportion of variance in the trait values.

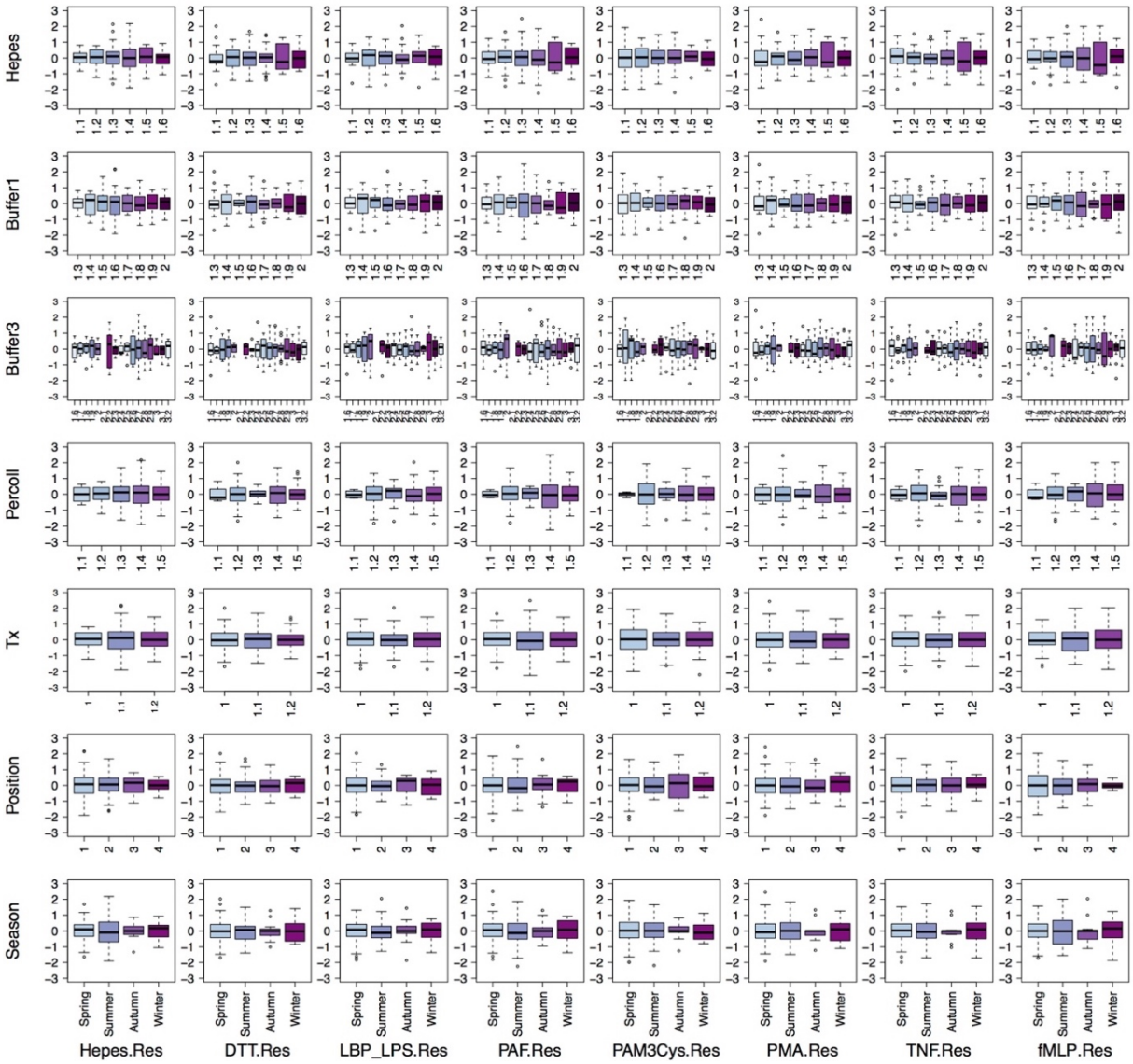

Figure 3.10: Correction of known batch effects
Boxplots show the residuals stratified by covariate levels. The residuals are shown from linear regression models with all of the listed covariates were applied to each trait to remove variation due to changes in these factors. season. This demonstrated that the means of each level were equalised even for Buffer 3 for which there were 17 batches.

Phenotype correlation: In order to investigate whether there was evidence of any similarity between phenotype traits, I used unsupervised clustering analysis by calculating Pearson correlations between all pairwise comparisons between residualised trait values. The R package, pheatmap, was used to plot the heatmap demonstrating clusters between particular traits.

3.2.3 Genetic analysis and integration with epigenomic datasets

Genetic data: This cohort consisted of a mix of individuals either from the Blueprint consortium or the Cambridge BioResource (CBR) (http://www.cambridgebioresource.org.uk/). If individuals were part of the Blueprint consortium, whole-genome sequence (WGS) data was available and was analysed as part of this project (Chen et al., 2016a). For CBR individuals, genotypes were available from the HumanOmniExpress-12v1 chip, the HumanCoreExome-12v1-0 and HumanCoreExome-12v1-1 genotyping chips, imputed using the combined reference panel of UK10K and 1000G Phase 1. Individuals were analysed as part of the large cohort (more than 3000 individuals) by Heather Elding, following all of the standard genotype QC procedures (Anderson et al., 2010). A logistic regression of SNPs with genotyping batch was performed to remove variants with discordant allele frequencies across batches. For this study, only variants that were shared between the WGS and genotyping datasets were used in downstream association analysis. All alignments and analyses in the Blueprint EpiVar project were carried out using GRCh37/hg19 and GENCODE v15 (Harrow et al., 2012). The analysis of the WGS data was performed as part of the Chen *et al.* (2016) study (Chen et al., 2016a).

Genetic association: The residuals of each trait were standardised and used as phenotypic traits in downstream genetic association analyses. Single variant association tests were performed using SNPTEST v2.4.0, and tested the association for each variant with each trait using an additive model (-frequentist 1). For each residualised trait, y_i and variant genotypes, x_i, a linear model $y_i = \beta_0 + \beta_1 x_i$ was fitted for $i = 1,2,3,\ldots,n$, where n is the number of individuals in the cohort. Genotype dosages were used (-method expected) to account for genotype uncertainty and expressed as the probability of each SNP genotype (AA, AB, and BB) per individual with 1 being most certain and NA for missing. Default quantile normalisation was disabled using the option -use_raw_phenotypes as the input phenotypes values were standardised at the stage of preparing the sample file. Variants with a MAF of less than 1% were excluded given the lack of statistical power to detect rare variant associations in this particular cohort.

Visualisation: Manhattan and QQplots were produced either using custom in-house scripts or using the QQMAN R package (Turner, 2014). Locus zoom plots were generated using the

online tool (Pruim et al., 2010). Promoter-capture HiC plots were visualised using the Capture HiC plotter (CHiCP) (https://www.chicp.org) (Schofield et al., 2016).

Significance threshold: All variants meeting the standard-genome wide association threshold of 5×10^{-08} were identified. 5×10^{-08} is an appropriate testing thresholds for common variants in a European population, as tested here. In addition, neutrophil biological and genomic data were used to annotate these associations (see below) and therefore for suggestive associations that could be evaluated in a biological context, a threshold of 1×10^{-07} was applied.

Investigation of biological mechanism: I assessed whether significant or suggestive variants overlapped with any epigenomic or similar biological data in order to make predictions of possible variant functionality. I used ChIP-seq data from undifferentiated and differentiated HL60 cells, data from primary neutrophils from the BLUEPRINT consortium and epigenomic data including CTCF, PU.1 C/EBPβ, H3K27me3 (repressive) and H3K4me3 (active transcription) from primary neutrophils as part of an unpublished dataset (Stephen Watt, manuscript in preparation) (all described in Chapter 2). Further, I used binding data from undifferentiated HL60 cells including P300 (enhancer co-factor), C/EBPε (TF) and cohesin subunits SA1 and Rad21 (cis-regulatory module protein) that was collected within the Soranzo team by myself and Stephen Watt. I used the bedtools analysis suite (bedtools version 2.23.0) with the -intersect option to assess intersection of genetic variants and molecular features. Promoter-capture HiC data from primary neutrophils, which describes long-range interactions between genomic locations, was used to identify potential target genes of significant variants (Javierre et al., 2016). In addition, the potential effects on neutrophil gene expression of function-associated variants were assessed using RNA-seq data as part of the Blueprint consortium (Chen et al., 2016a). Rare or lower-in-frequency variants were not tested within the BLUEPRINT study, therefore to evaluate the function of rare/low-frequency variants, associations were tested using the RNA-seq gene expression data in FPKM.

Replication cohort: To confirm neutrophil function effects identified in the Cambridge discovery cohort, together with our collaborators, we established a cohort of healthy individuals in the Netherlands at Sanquin Research, University of Amsterdam (Sanquin cohort). Samples were genotyped at the Wellcome Trust Sanger Institute using the Illumina Human CoreExome Beadchip (coreex24) array. All genetic analysis for this cohort was carried out by Klaudia Walter (WTSI), but is summarised briefly here. A standard quality control protocol was implemented that included identity (≥ 0.9), duplicate (≤ 0.98) and gender checks (males ≤ 0.005, females ≥ 0.174), as well as a minimal call rate (≥ 0.95) and no

excess autosomal heterozygosity (three standard deviations). 157 donors were genotyped in two batches (83 donors in the first and 74 donors in the second batch). In total eight donors failed the heterozygosity threshold and three donors failed the duplicate threshold. Additionally, a principal component analysis (PCA) was carried out together with HapMap3 samples which identified 14 population outliers, of which eight samples had also failed the heterozygosity threshold. In total 17 samples were excluded from further analysis. Samples were imputed using the Haplotype Reference Consortium (r1.1) using the EAGLE2+PBWT pipeline. The samples were processed with ethical consent approved by the WTSI Human Materials and Data Management Committee, reference 16/042 and titled: “Genetic variation in neutrophil cellular function- Biobank sample donors of Sanquin Research”.

Genotype validation: We identified a genome-wide significant association for a low-frequency locus (rs116811177/rs115109232, MAF = 2%, Figure 3.14). Given the low-frequency of these SNPs, we used Sanger sequencing with probes designed for rs116811177 and rs115109232 to confirm the heterozygous genotypes for the five individuals in the discovery cohort association (Figure 3.15). The genotyping assay was designed by Agena Bioscience using the MassARRAY® System with the iPLEX® chemistry.

3.3 Results

3.3.1 Phenotype Correlation

This study describes the first large-scale exploration of neutrophil adhesion, degranulation and respiratory burst from a predominantly healthy cohort, which enables a direct comparison of the relationship between these responses. In total, 29 traits were assessed across three assays and 12 different stimuli (Table 3.2). For adhesion, eight different stimuli were used and the final response measured as a single relative fluorescence unit (RFU). For respiratory burst and degranulation, four and two different stimuli were used respectively. Traits were calculated from the response distributions for all donors measured for either 120 or 60 cycles for each individual (Table 3.2).

I implemented unsupervised clustering analysis using the Pearson correlation between each pairwise residualised trait comparison to investigate similarities between the different neutrophil functions (Figure 3.11). Interestingly, two higher order clusters were observed, one between respiratory burst and degranulation responses and the other of adhesion responses. Mean correlations within these clusters revealed that the correlation between degranulation and adhesion responses was particularly low (mean r = 0.068, SD = 0.052). By contrast, the average correlation between respiratory burst traits and degranulation traits was 0.148 (SD = 0.093). However, the correlation between adhesion traits and respiratory burst traits was higher than that between degranulation and adhesion (r = 0.144, SD = 0.100). The correlations within responses of the same assay were all above 0.48 with the highest between degranulation traits (r =0.732, SD = 0.187).

There was a negative correlation between both time to particular RFU respiratory burst traits (PMA time to reach an RFU at 40000 cycles and STZ time to reach an RFU of 30000 cycles) and the rest of the respiratory burst responses. A high responder will reach a high maximum slope or RFU in a shorter time period due to the fast reaction response. These traits also clustered with the rest of the adhesion responses. The biological reason underlying the slight correlation of these time traits with adhesion responses is unclear.

The adhesion HEPES response was clustered with the rest of the adhesion responses, which could suggest that this condition demonstrates a degree of pre-stimulated activity in this particular function, which has been observed primarily in the adhesion assay over respiratory burst and degranulation by our collaborators (personal communication, Anton Tool).

The higher observed correlation and similarity between degranulation and respiratory burst responses may reflect activation of shared components of biological pathways or that certain

stimuli lead to a concomitant activation of multiple biological pathways culminating in the activation of multiple neutrophil functions.

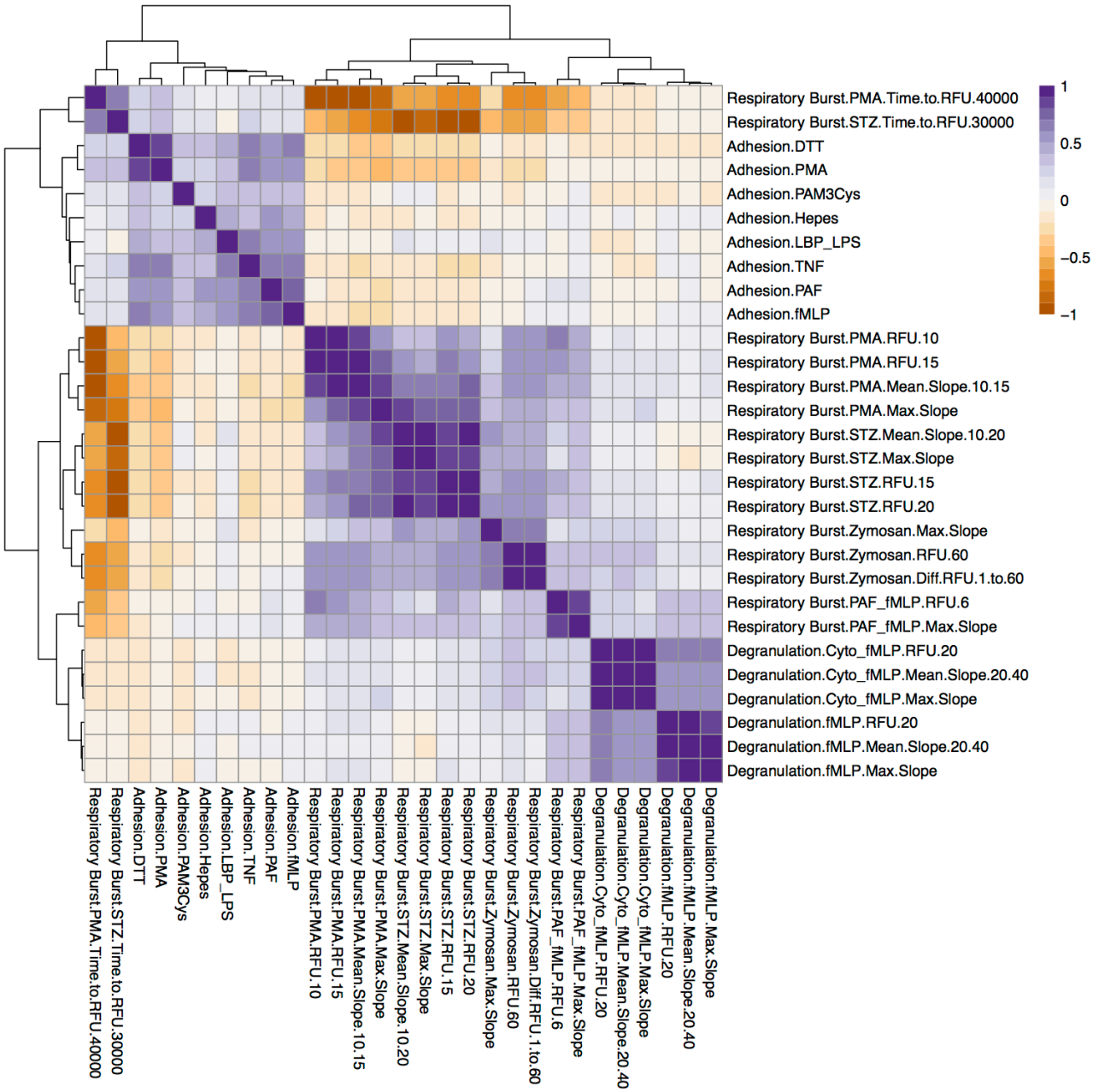

Figure 3.11: Correlation of neutrophil function phenotypes
Heatmap shows the correlation between standardised residuals from all traits and stimuli used in genetic association analyses. The Pearson correlation between all traits was calculated and used in unsupervised clustering analysis to assess the relationship between neutrophil functional responses. Respiratory burst and degranulation responses correlated more closely than to adhesion response with the exception of the response to HEPES (which should represent unstimulated responses) and the time to a specific RFU response.

3.3.2 Genetic variants associated with inter-individual variation in neutrophil function

I used the standardised residualised values for the 29 traits described above in independent single variant genome-wide association tests. Just over six million SNPs after filtering for variants below 1% MAF were tested for association with each trait. We estimated that this study was powered to detect common variants of moderate to high effect size and low-frequency variants with standard beta estimates of approximately 3 SD (Supplementary Figure 3.2).

I identified two SNPs reaching genome wide significance that were associated with respiratory burst of neutrophils stimulated with PAF and fMLP (p value < 5×10^{-08}, Table 3.3, Figures 3.12-3.14). The two low-frequency SNPs, rs116811177 (EA = G, EAF = 0.02, beta = 2.92, SE = 0.398, p value = 2.39×10^{-11}) and rs115109232 (EA = A, EAF = 0.02, beta = 2.92, SE = 0.398, p value = 2.39×10^{-11}), are perfectly correlated with r^2 of 1 (1000G). There were five individuals in the heterozygote state that demonstrated an increase in the respiratory burst response (Figure 3.15). No other genetic variants reached genome-wide levels of significance with any of the other functional traits. There were six variants that were associated at the suggestive p value threshold (p value < 1×10^{-07}, summarised in Table 3.3). All of these SNPs were low frequency (MAF < 5%) except one that was associated with adhesion response stimulated by PMA (rs57784565, p value = 8.59×10^{-08}, MAF = 7.6%). The remaining variants were all associated with respiratory burst of neutrophils stimulated with PAF and fMLP.

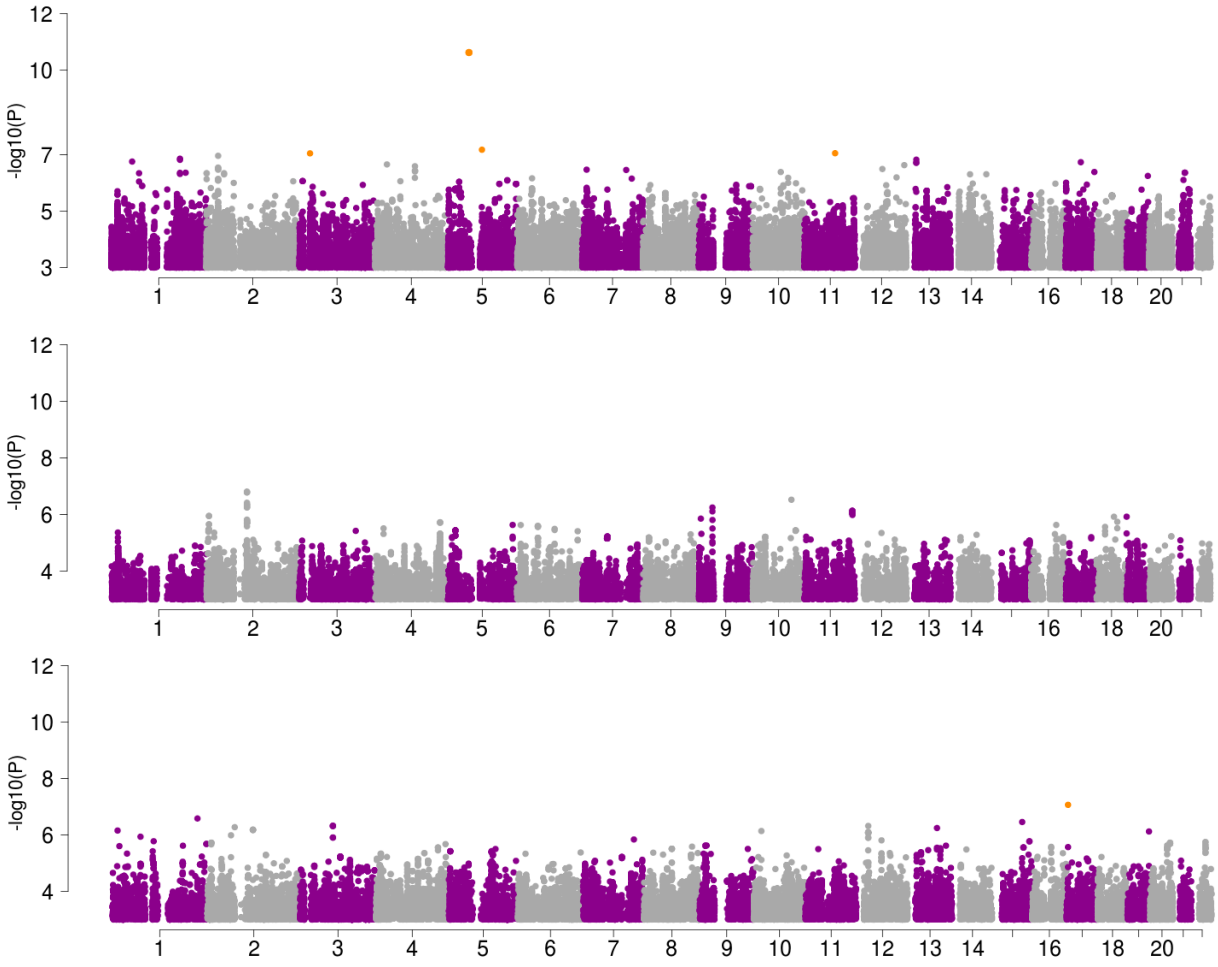

Figure 3.12: Association results for neutrophil function responses
Manhattan plot showing all variants associated with all traits at a p value threshold of 1 x 10^{-03} or less. A) Respiratory burst-associated variants, with a genome wide significant locus signal on chromosome 5. B) Degranulation-associated variants showed a lower number of variants associated at the threshold than respiratory burst but possible suggestive signals on chromosome 2 and 9. C) Adhesion-associated variants with a signal that just missed the significance threshold (approximately 9.0 x 10^{-08}) on chromosome 17. Responses for all the conditions and traits were combined into one Manhattan plot per assay. Variants associated with a p-value threshold of less than 1.0 x 10^{-07} are highlighted in orange.

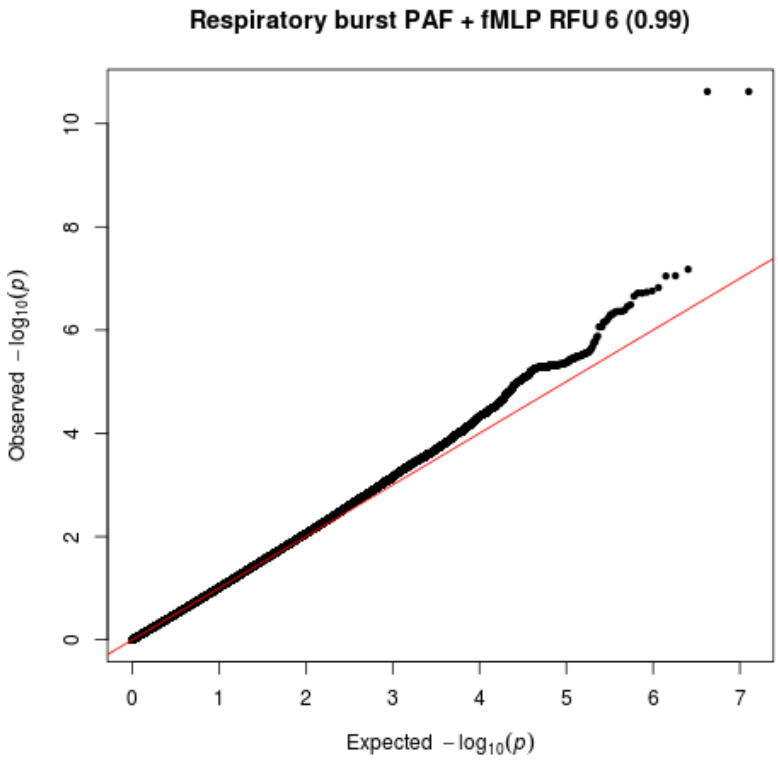

Figure 3.13: QQ plot of the respiratory burst PAF and fMLP RFU at 6 cycles response
Expected -log10(p value) calculated using a uniform distribution against the observed -log10(p value) from the function single variant association test. The deviation from the expected line demonstrates that genome-wide significant variants were more associated with the trait than expected by chance. The genomic control factor, lambda, was 0.99, suggesting there was no evidence for population stratification in this sample cohort.

rsID	Trait	chr:pos	EA:OA	P value	Beta	SE	MAF	Annotation	PcHiC	Protein Expression	Epigenome
rs116811177	Respiratory burst PAF + fMLP RFU 6	5:55597870	G:T	2.392×10^{-11}	2.92	0.398	0.020	Upstream, RNU6ATAC2P	MAP3K1	Expressed SV neu	
rs115109232	Respiratory burst PAF + fMLP RFU 6	5:55599891	A:G	2.392×10^{-11}	2.92	0.398	0.020	Intergenic	MAP3K1	Expressed SV neu	
rs147669752	Respiratory burst PAF + fMLP RFU 6	5:89571908	G:A	6.649×10^{-08}	2.82	0.491	0.016	Intron RP11-61G23.1	LINC00461 CTC-467M3.1		
rs117183808	Respiratory burst PAF + fMLP RFU 6	11:80312077	T:G	8.856×10^{-08}	2.97	0.523	0.012	Intergenic			
rs7623696	Respiratory burst PAF + fMLP RFU 6	3:28332261	T:A	8.956×10^{-08}	2.12	0.373	0.03	Intronic CMC1			H3K4me1
rs57784565	Adhesion PMA	17:3635489	A:G	8.596×10^{-08}	1.31	0.231	0.076	Intronic ITGAE	ZZEF1	Expressed PM neu	H3K4me1

Table 3.3: Function-associated variants across all assays
Table summarising statistics and annotations of variants reaching a suggestive p value threshold of 1.0×10^{-07}. Genome-wide significant variants, rs116811177 and rs115109232 are low-frequency and associated with respiratory burst. For each variant, association statistics including p-value, beta, standard error of beta (SE) and minor allele-frequency (MAF) (in this cohort) are listed. Variant effect predictor (VEP) was used to annotation variants (McLaren et al., 2016). A range of epigenomic data was used to annotate potential function to these variants (Materials and Methods). PcHiC data describes neutrophil-specific promoter-capture HiC data. If a variant intersects with either fragment end of a long-range interaction the corresponding gene of the other end is listed. Intersection with histone modified regions or transcription factor binding regions as assayed by ChIP-seq is also listed. The protein expression column refers to a study that compared proteins expressed on the plasma membrane (PM) or secretary vesicles of human neutrophils (Uriarte et al., 2008).

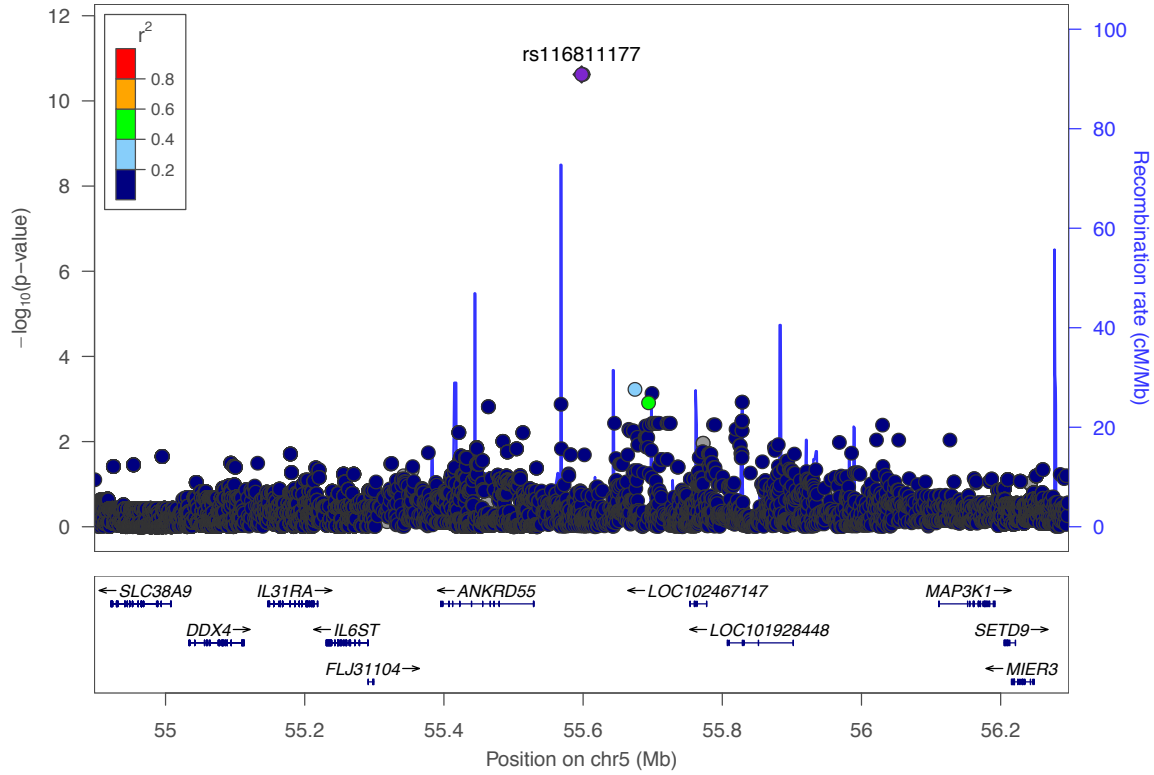

Figure 3.14: Genic location of the most significant signal associated with neutrophil respiratory burst

Regional plot of association for variants associated with respiratory burst RFU 6 in the region (+/- 700 kb) of the lead variants, rs116811177/rs115109232.

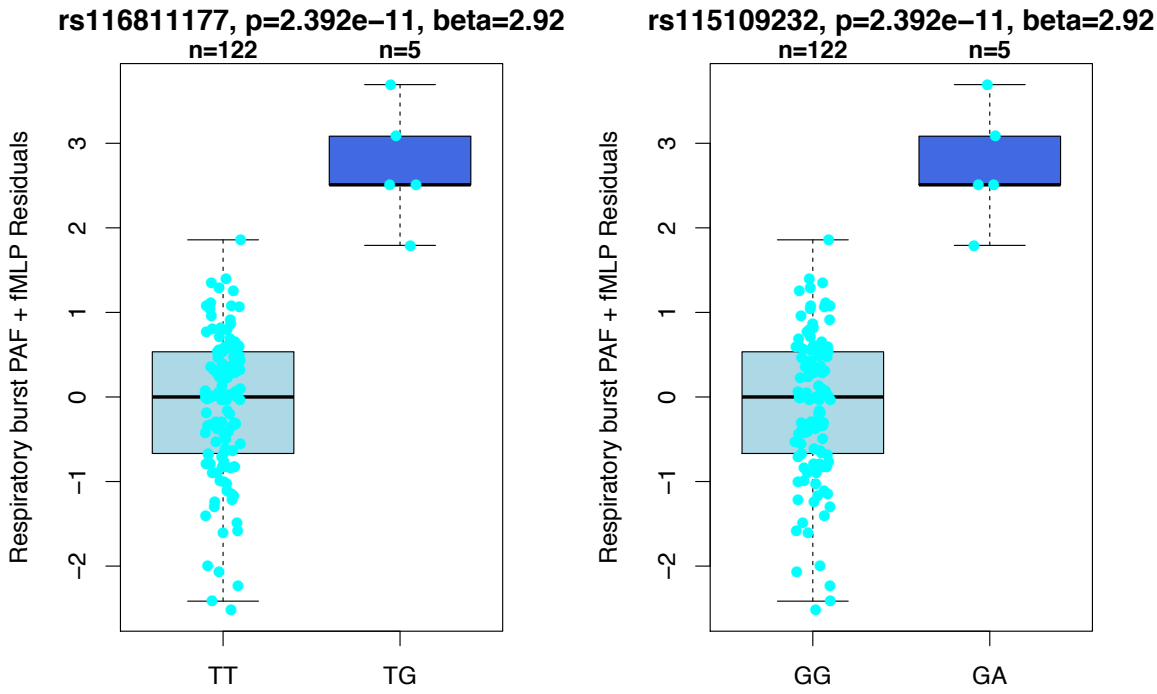

Figure 3.15: rs116811177/rs115109232 increases respiratory burst response after neutrophils are stimulated with PAF and fMLP

Residualised values of the respiratory burst response stimulated by PAF and fMLP at RFU 6 cycles are stratified by genotype of the two SNPs of the top genetic signal associated with this trait. Trait values of each individual are demonstrated as light blue dots.

3.3.3 Functional annotation of the PAF & fMLP respiratory burst rs116811177/rs115109232 locus

Figure 3.14 shows that the rs116811177/rs115109232 SNPs are intergenic, complicating identification of functional mechanism. In order to identify potential target genes, I used a range of publicly available datasets including gene expression QTLs (eQTLs) and promoter capture HiC data to query long-range interactions (Ward and Kellis, 2012, Chen et al., 2016a, Javierre et al., 2016).

Recently, it was demonstrated that complex-trait associated variants are enriched in regions of the genome connected through long-range chromatin interactions (Javierre et al., 2016). Potential distal gene targets of non-coding variants were identified using specific chromatin interaction data (Javierre et al., 2016). Therefore, to identify possible gene targets, I intersected variant positions (Table 3.3) with the fragment locations of promoter-capture HiC data from primary human neutrophils (Javierre et al., 2016, Schofield et al., 2016). I identified that both of the top most significant variants, rs116811177 and rs115109232, overlap a fragment that connected these variants to the promoter (and gene body) of two protein-coding genes; *MAP3K1* and *AC022431.2* as well as an interaction that connected these variants to the promoter of the *MIER3* gene (Javierre et al., 2016) (Figure 3.16). The latter gene, *AC022431.2*, which has no known genic annotation, was lowly expressed in neutrophils (median FPKM < 3 (Chen et al., 2016a)). In contrast, *MIER3* (the mesoderm induction early response protein 3) and *MAP3K1* (mitogen-activated kinase kinase kinase 1) were both expressed in neutrophils with *MAP3K1* being the most highly expressed (> 9 median FPKM).

Having identified possible gene targets, I next investigated whether the SNPs were associated with differential expression of these genes. I queried both publicly available gene expression data (HaploReg v4.1 (Ward and Kellis, 2012) and the primary human neutrophil RNA-seq data from the BLUEPRINT cohort (Chen et al., 2016a). I used data from unstimulated cells, rather than stimulated, as the PAF & fMLP respiratory burst response was known to be a fast reaction (minutes) rather than over several hours. Therefore, any gene expression effect associated with these SNPs would have to be present in unstimulated neutrophils. The low-frequency rs116811177/rs115109232 SNPs were not tested as part of the BLUEPRINT, therefore I retrieved the normalised FPKM gene expression values and the genotypes of individuals discordant at these SNPs in order to identify any evidence of gene expression effects. Within this cohort, nine individuals were heterozygous for rs116811177 or rs115109232. I also considered genes in the proximal region with a median neutrophil gene expression value greater than 3 FPKM and those with a known function. The included: *IL31RA, IL6ST, ANKRD55, FLJ31104, MAP3K1, SETD9, MIER3, SLC38A9* (Figure 3.14). I

did not detect any significant differences in gene expression for any gene including MAP3K1, despite the significant long-range chromatin interactions (Figure 3.16).

I did not observe any further epigenomic intersections with the rs116811177/rs115109232 SNPs and other datasets such as histone modification peaks or transcription factor binding (H3K4me1, H3K27ac, H3K4me3, PU.1, C/EBPβ, C/EBPε, cohesin) using the bedtools intersect function (Materials and Methods).

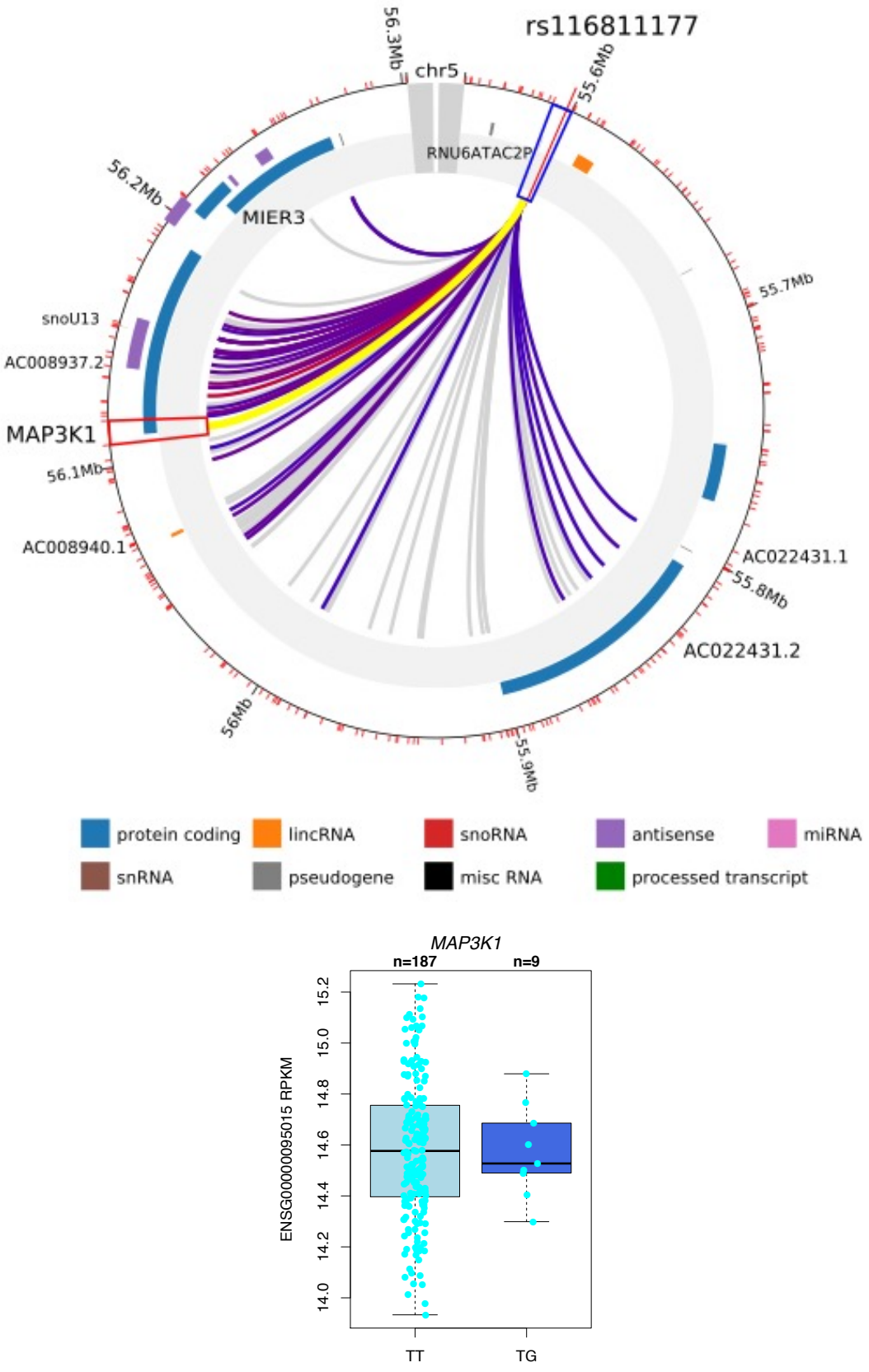

Figure 3.16: Functional annotation of the rs116811177/rs115109232 (*MAP3K1*) locus
Top panel depicts long-range interactions of the rs116811177/rs115109232 locus with various genes (labelled). Significant neutrophil interactions are shown in purple, with the *MAP3K1* promoter interaction in yellow with interaction score of 12 (> 5 is a significant interaction over background) (Cairns et al., 2016, Dryden et al., 2014). This figure was produced using the Capture HiC Plotter (CHiCP) accessed in July 2017 (Schofield et al., 2016). The bottom panel shows there is no evidence of differential *MAP3K1* gene expression with respect to genotype of the rs116811177 SNP.

3.3.4 Replication of the rs116811177/rs115109232 locus in an independent cohort

In order to investigate whether we could replicate the association at the rs116811177/rs115109232 locus, we established an independent cohort of healthy individuals from Sanquin Research, University of Amsterdam, the Netherlands (Materials and Methods). The DNA from healthy individuals was genotyped at the Wellcome Trust Sanger Institute and the final number of individuals in this cohort was 140 (Materials and Methods).

We aimed to use this cohort to replicate the increase in respiratory burst response within donors that were either heterozygous or homozygous for the effect allele of the rs116811177/rs115109232 locus. We decided that individuals of all three genotypes would be recalled and tested on the same day, in part to mitigate against the observed source of co-variation that can be introduced in measuring function on different days. Within the Sanquin cohort, there was one individual homozygous for the increasing PAF/fMLP respiratory burst effect allele (GG) and five heterozygous individuals. The homozygous increasing (GG) individual was recalled on the same day as individuals of either the heterozygous (GT) and homozygous decreasing (TT) genotype. These experiments are technically complex to perform and therefore a maximum of six individuals could be recalled on one day. The experiments were performed at Sanquin Research by Anton Tool.

Figure 3.17 shows the initial replication effort where the respiratory burst response was measured in nmol H_2O_2/min per million neutrophils, where the raw measured RFU was converted to nmol using a calibration curve of known concentrations of H_2O_2. A higher concentration of H_2O_2 corresponds to a higher RFU and therefore higher response that could be compared to the Cambridge discovery cohort. Figure 3.17 shows a higher PAF fMLP respiratory burst response in a homozygous increasing individual (rs116811177, GG) compared to an individual of TT genotype (non-carrier, Figure 3.17). No similar difference in response was observed for the other conditions tested (Figure 3.17). The high PAF and fMLP response associated with increasing copies of the G allele was consistent with the observations of the effect of this locus in the Cambridge discovery cohort (Figure 3.15).

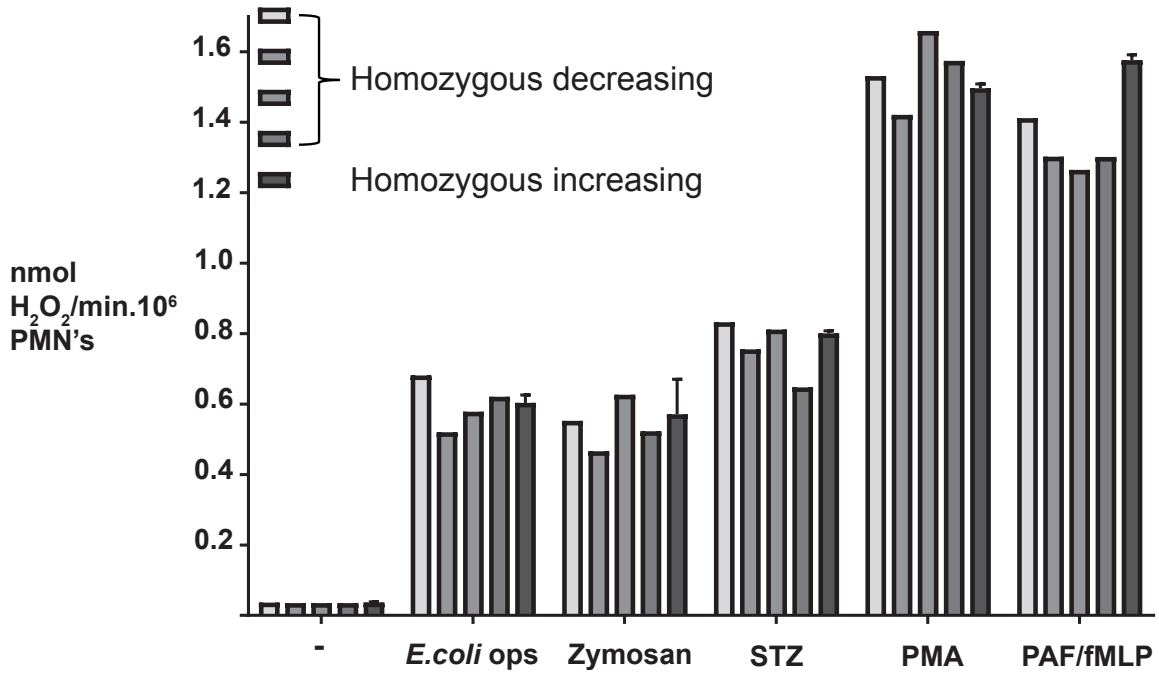

Figure 3.17: The rs116811177/rs115109232 (*MAP3K1*) locus in an independent cohort
Neutrophil function responses for different stimuli and donors (bars) as measured at Sanquin Research by Anton Tool. The different bars are coloured based on the genotype of the rs116811177/rs115109232 locus. Genotype groups refer to the predicted direction of PAF/fMLP respiratory burst effect from the original Cambridge cohort (Figure 3.15). A similar increase in PAF and fMLP response is seen in the homozygous-increasing individual compared to the non-carriers. The response is measured in nmol H_2O_2 per minute per million neutrophils by conversion using a calibration curve. Error bars on the plots demonstrate the difference between technical replicates. PMNs = polymorphonuclear neutrophils. Figure adapted from Anton Tool.

3.4 Discussion

We demonstrated, through thorough exploration and visualisation, how functional phenotypes are highly complex in both acquisition and sensitivity to environmental and technical factors, although good agreement was observed between technical replicates. I observed that after applying linear regression, the residuals, which contain the remaining variation after removal of specified sources of co-variation, did not show clear batch stratification (Figure 3.10). Some neutrophil responses were affected by external factors such as season (Figure 3.9, Supplementary Figure 3.1).

Previously the effect of annual seasonality on cytokine production from stimulated PBMCs and macrophages has been shown in the Human functional genomics project (Ter Horst et al., 2016). In this study, the authors also tested the effect of season on cytokine immune responses using a linear regression approach and demonstrated that the production of TNFα, IL-1β and IL-6 are highest in the summer. Conversely, the anti-inflammatory alpha-1-antitrypsin (AAT) production was highest in the winter. AAT seasonality was inversely correlated with the incidence of joint-disorder gout in a cohort of 800 patients. AAT inhibits IL-1β corresponding to lower cell infiltration into mouse joints, potentially explaining how the drop of AAT increases the inflammatory environment leading to exacerbation of gout (Ter Horst et al., 2016). There is, therefore, precedence for the effect of season on immune responses. I observed that in most cases, neutrophil functional responses were lowest in winter. The biological reasons and physiological implications for this are unclear and could reflect seasonality or differences in environmental temperatures in experimental processing. The decreased inflammatory response in winter was in agreement with that observed by Ter Horst *et al.* (2016). In future, it would be interesting to investigate any available clinical data in order to assess any physiological correlations with this observation. In this study, the effect of season was removed using linear regression prior to genetic association tests.

Individual's age and gender did not have a large significant effect on most neutrophil responses as shown by the small R^2 values and non-significant p values from ANOVA testing (Figures 3.8-3.9). Previously, differences in neutrophil differential gene expression have been observed between males and females (Ecker et al., 2017). Genes with higher expression levels in females were enriched in immune response pathways but those increased in males were enriched in basic cellular processes, which the authors suggested could explain the higher incidence of autoimmune diseases in women. Therefore, gender (and age) effects could have an effect on some responses, but in comparison to experimental factors and season the R^2 estimates are lower. Indeed, gender was found to be a significant covariate for adhesion stimulated with TNF (p value = 3.9×10^{-03}), Pam3Cys (p

value = 0.029), LPS (p value = 6.6 x 10^{-04}) and fMLP (p value = 0.020) but was not significant for any degranulation or respiratory burst traits.

Encouragingly, after correction for sources of co-variation, the correlation of trait measurements seemed to recapitulate aspects of previously observed biological relationships between these functional responses. Degranulation and respiratory burst traits formed a separate cluster compared to adhesion responses, which perhaps suggests the former biological processes share biological pathways or could be co-regulated. Degranulation responses and adhesion responses showed the lowest correlation of all comparisons. In the degranulation assay, we stimulated neutrophils with the soluble stimulus, fMLP. When using soluble stimuli, we know that DQBSA is cleaved by the elastase and Cathepsin G proteases, which are released into the neutrophil supernatant (Anton Tool, personal communication). These two proteases are contained in the azurophilic granules, which are known to be released at later stages in the neutrophil activation process (Table 3.1) (Amulic et al., 2012). Therefore, this may explain the low correlation with adhesion processes, which occur earlier in neutrophil activation.

There is evidence for adhesion-stimulated degranulation (and ROS production) in an "outside-in" signalling process mediated by integrins. Integrin interaction with surface-bound anti-β2 and anti-β3 monoclonal antibodies alone, without inflammatory stimulus activation, induces neutrophil respiratory burst (Berton et al., 1992, Lowell et al., 1996, Berton and Lowell, 1999). Indeed, regulation of these processes is required to prevent aberrant inflammation. An initial inhibition of ROS production following neutrophil adherence to the extra-cellular matrix proteins such as fibronectin, fibrinogen and laminin, acts as a mechanism to prevent inappropriate tissue damage as these cells migrate towards inflamed tissues (Zhao et al., 2003, Al Laham et al., 2010). However, currently, the full pathways involved in these responses are not yet known so further experimental evidence is required to thoroughly interpret these correlations.

We were able to sufficiently correct for *known* technical and biological sources of covariation. However, the experimental design of this study did not enable correction for unknown sources of covariation or day-to-day effects. Studies with higher sample sizes have demonstrated a vast number of factors that lead to variation in trait values, for example in the large GWAS (N ~ 174000) of mature blood cell counts co-variation sources included time of measurement, menopausal age or smoking status (Astle et al., 2016). However, the detection of these effects in our study is limited by the low sample numbers, low number of traits and low number of individuals measured in one day (owing to the technical complexity

of the assays). In most cases (56%), only one donor was measured per day, prohibiting approaches such as within-day standardisation to correct for day-to-day changes.

These issues highlight the importance of extensive exploration of association signals using other sources of biological data. In the original Cambridge discovery cohort, we identified a single genetic locus of two highly correlated, low-frequency SNPs rs116811177 (EA = G, EAF = 0.02, beta = 2.92, SE = 0.398, p value = 2.39×10^{-11}) and rs115109232 (EA = A, EAF = 0.02, beta = 2.92, SE = 0.398, p value = 2.39×10^{-11}) reaching genome-wide significance associated with the fMLP/PAF respiratory burst response. There were five heterozygous donors for the rs116811177/rs115109232 (*MAP3K1*) locus predicted have an increased respiratory burst response. Four of these donors had genetic data available from whole-genome sequencing (mean PAF + fMLP RFU 6 residualised trait value = 2.12) while the remaining donor had data available from a genotyping chip (PAF + fMLP RFU 6 residualised trait value = 0.93). We identified that two of these donors had been assayed on the same day (26th January 2015). I identified that there were no reagent batch changes between the previous days and when these two donors were measured and both donors were female. This suggests that the increased responses were not due to any known sources of covariation. Given this limitation in our study design, we designed the Sanquin replication study (described below) so that donors of different genotypes will be measured on the same day, removing the possibility of day-to-day variation in affecting these responses.

Despite these limitations, there is evidence that the proposed target gene of this locus, *MAP3K1*, is important in the respiratory burst response. MAP3K1, also known as MEKK, is a signalling kinase that activates the ERK and JNK pathways to coordinate downstream cellular processes such as proliferation, differentiation and stress (Chadee et al., 2002). It has also been observed that MAP3K1 is activated in response to fMLP in primary neutrophils, which is the same chemoattractant stimulating the respiratory burst response to which the rs116811177/rs115109232 is associated (Avdi et al., 1996). This could indicate that, through an effect not mediated by gene expression, the variants influence *MAP3K1* functioning in the respiratory burst response. For example, the phosphorylation status of *MAP3K1* could be altered as a function of genotype, which could be experimentally measured and is under discussion as future work in the replication cohort. Further annotations provided by the HaploReg resource (Ward and Kellis, 2012) also provided evidence that this region may be important in cellular signalling. The signalling compound, c-FOS has been shown in HUVEC cells to be bound at the r116811177 variant site using ENCODE ChIP-seq approaches. The second variant at this locus, rs115109232, is predicted to disrupt a Myc transcription factor motif, which is another important signalling molecule.

Subsequent to this analysis, it was identified that the Buffer 3 used in neutrophil preparation contained citrate, likely to facilitate measurement of full blood count in the Sysmex analyser. Citrate acts to chelates extracellular calcium, which could reduce calcium influx and in turn diminish neutrophil functional responses. Subsequent experimental repeats of these assays with and without calcium in the buffer demonstrated a decrease in functional responses. This could result in a decrease in power to detect signals and places greater importance on fully replicating the genome-wide significant locus identified in the Cambridge discovery cohort.

In conclusion, despite the small number of samples, this study showed that GWAS of neutrophil functional traits could provide a means for discovering novel regulatory regions controlling immune responses, in this particular case of the neutrophil fMLP-respiratory burst response. However, the use of such datasets to annotate disease-risk loci that could be explained by dysregulated neutrophil function would require greater sample sizes as we were limited in power in this present study to broadly annotate disease-risk loci.